R. & M. No. 3385

MINISTRY OF AVIATION

AERONAUTICAL RESEARCH COUNCIL
REPORTS AND MEMORANDA

Transonic Tunnel Tests on a 6% Thick, Warped 55° Sweptback-Wing Model

By A. B. HAINES, B.Sc., and J. C. M. JONES, B.Sc.(Eng.)

LONDON: HER MAJESTY'S STATIONERY OFFICE
1965
PRICE 17*s.* 0*d.* NET

Transonic Tunnel Tests on a 6% Thick, Warped 55° Sweptback-Wing Model

By A. B. HAINES, B.Sc., and J. C. M. JONES, B.Sc.(Eng.)

*Reports and Memoranda No. 3385**

September, 1960

Summary.

Tests have been made in the A.R.A. 9 ft × 8 ft Transonic Tunnel on a model having a 6% thick, 55° sweptback wing with a warp distribution designed to give a constant spanwise C_L – distribution and a triangular chordwise load at $C_L = 0{\cdot}15$, $M = 1{\cdot}2$. The wing-body junction was designed according to supersonic area rule for this Mach number.

The results can be considered as encouraging. Subcritical-type flow is maintained over most of the wing under the design conditions. The margins in both Mach number at the design C_L and in C_L at the design Mach number before the start of any serious supercritical increase in drag or before the appearance of any significant shock-induced separations are of the order of 0·05. Major changes in the pitching-moment characteristics are even further delayed.

At subsonic speeds and low C_L, K is near 1·2 while at the design conditions, the approximate value from the experimental results is $K = 1{\cdot}55$ as compared with a theoretical prediction of $K = 1{\cdot}33$.

The results suggest that it is unlikely that there was a sizeable sweep factor on the wing skin-friction drag although no firm conclusion can be drawn about this.

Translating the wing-fuselage drag results to a typical full-scale Reynolds number, L/D for $C_L = 0{\cdot}15$ varied from about 12 at $M = 1{\cdot}2/1{\cdot}25$ to about 9 at $M = 1{\cdot}4$. Some incremental drags are also given for a particular fin-tail unit but these are not necessarily representative of a full-scale aircraft since the fin-tail unit was designed specifically to suit the requirements of a subsequent free-flight test of the model.

Finally, the report includes some data showing the downwash at the tail position both for this model and for a corresponding model having a symmetrical, untwisted wing.

LIST OF CONTENTS

* Replaces A.R.A. Wind Tunnel Note No. 25—A.R.C. 22 466.

LIST OF CONTENTS—*continued*

Section

LIST OF ILLUSTRATIONS

Figure

---

1. *Introduction.*

The design of a transport aircraft to fly at low supersonic speeds such as $M = 1{\cdot}15 - 1{\cdot}2$ is considered in Ref. 1. It is shown that it may be possible to achieve attractive values of lift/drag ratio at these speeds by designing the layout so that there is essentially subcritical-type flow over the wing surface. This means choosing the wing sweepback and thickness/chord ratio such that at the most, only weak shock waves will be present on the corresponding infinite sheared wing at the design C_L and Mach number and then, waisting the wing-body junction and devising a warp distribution across the span so as to maintain a uniform isobar pattern on the actual sweptback wing.

An extensive programme of tests has been undertaken in various wind tunnels and also by the free-flight technique to investigate the aerodynamic characteristics of aircraft configurations of this type. Many of the models have used the sweptback-wing planform proposed in Ref. 1, viz. a 55° sweptback wing of aspect ratio 3·4, basically untapered but with a curved leading edge over the outer half of the semi-span such that at the tip, the leading edge is tangential to the free-stream direction. For the free-flight models, the thickness/chord ratio could not be reduced below 6% because of structural considerations and so this value was chosen for a series of models tested with alternative body shapes and with either a symmetrical or a warped wing. The warp was designed for $C_L = 0{\cdot}15$ since on the crude estimates of Ref. 1, the combination of 55° sweepback, 6% thickness/chord and $C_L = 0{\cdot}15$ should be consistent with a cruise Mach number of $M = 1{\cdot}2$.

The warped 55° sweptback free-flight model was first tested in the Aircraft Research Association 9 ft × 8 ft Transonic Tunnel and the present report gives the results of these tests. The model was tested both as a simple wing-fuselage combination and with the fin-tail unit subsequently used in the free-flight tests. Lift, drag and pitching moment data were obtained and the downwash at the tailplane was deduced from the pitching-moment values for the model without tail and with the tail at four alternative settings. In addition, the report also includes some downwash data obtained with a yawmeter comb mounted in the tail position behind another model fitted with a corresponding symmetrical wing. Unfortunately, no drag data were obtained with this second model.

Some pictures are included of the oil flow over the model both under the design conditions and at certain more extreme conditions. These serve to demonstrate that subcritical-type flow is maintained

over most of the wing under the design conditions and that adequate margins exist before any strong shock waves are observed. Apart from these oil-flow pictures, most of the general interest in these results will centre on the drag data. The report compares these both with theoretical predictions for this particular design and with the values that have been fed into various project analyses. Later, they will be used for comparison with the results of other tests in the A.R.A. tunnel on a model having a wing of the same planform but with a thickness/chord ratio 4·5% rather than 6% and warped for a design C_L of 0·25 rather than 0·15. The calculations in Ref. 1 suggested that these two combinations of thickness/chord ratio and design C_L should correspond to about the same cruise Mach number ($M = 1·2$) although later calculations have now indicated that the 4·5% thick, $C_L = 0·25$ wing should more properly be considered as an $M = 1·15$ design. The tests on the thinner wing were much more comprehensive than those reported here for the 6% thick model; in particular, they included detailed pressure plotting at several stations on the wing. The thinner model is mentioned here because some of the thoughts contained in this report as to the reasons for the performance of the 6% thick model were inspired by a knowledge of the pressure-plotting results on the other wing.

The drag results obtained with the complete model including the fin-tail unit are not necessarily of such general interest. This fin-tail unit was designed specifically to suit the requirements of the subsequent free-flight tests and no attempt was made to design an area-rule layout in this respect; the tailplane is a simple tapered sweptback wing with a 4% thick RAE 101 section while the fin section is merely hexagonal. Hence there are several reasons why the drag of this particular fin-tail unit could be relatively large.

2. *Description of Model Design.*

A half general arrangement of the warped-wing model in plan view and in side elevation is given in Fig. 1a.

The wing has an aspect ratio of 3·40 and a basic sweepback of 55°. Over the outer half of the semi-span, the leading edge is curved and at the extreme tip it is tangential to the free-stream direction. This planform was suggested in Ref. 1 as a simplification of the type calculated by Brebner[2] to give a uniform distribution of C_L across the span.

The wing thickness/chord ratio was 6%. This value was dictated by structural considerations. These prevented a reduction to 4·5%, the value chosen for several wind-tunnel models in this programme. However, as already mentioned in the introduction, obtaining results for wings with two different thickness/chord ratios makes an interesting comparison and adds to the general store of knowledge. The thickness form was chosen as RAE 101.

The starting point for the body design was to choose an overall fineness ratio of 16 and a profile consisting of a von Kármán ogive for the forebody and afterbody with a cylindrical centre portion. The ratio of body diameter to wing root chord was 0·4. For the free-flight tests, the ogival afterbody was cut off to give a finite base and this had to be further modified for the tunnel tests in order to accommodate the sting; in the tunnel tests, the body behind the wing trailing edge was just a parallel circular cylinder (Fig. 1a).

To eliminate the wing-wave drag arising from wing-body thickness interaction effects, the basic body shape and the wing-body junction were modified using the supersonic area rule for a design Mach number of $M = 1·17$. This value was chosen in an attempt to give low wave drag at zero

lift over the Mach number range from $M = 1{\cdot}0$ up to say, $M = 1{\cdot}3$. Use of the supersonic area rule led to a bulging of the body just ahead of the wing leading edge as shown in Fig. 1b. In this particular design, the body diameter was not increased again near the wing trailing edge but was held constant downstream of about $0{\cdot}85 \times$ wing root chord. Another point to note is that circular cross-sections have been retained and so the body was modified both in plan view and in side elevation. The results in Ref. 3 provide some justification for the use of supersonic area rule in the present application. These results showed that for a wing of the present planform, the supersonic area rule appeared to be at least as good as any other method for reducing the drag at zero lift near the design Mach number.

In order to maintain subcritical-type flow at the design Mach number and non-zero lift, the wing had to be cambered and twisted. In this particular application, the wing warp was relied upon to give the full required effect; for some later models, the treatment has been shared between wing warp and an asymmetric body junction design, i.e. a different junction shape for the wing upper and lower surfaces. A design C_L of $0{\cdot}15$ was chosen on the basis of Ref. 1 to give, with the form of chordwise loading described below and with the thickness/chord ratio of 6%, a design appropriate to a cruise Mach number of $M = 1{\cdot}2$.

At the wing-root section ($y/s = 0{\cdot}128$), and over the region outboard of the forward Mach line from the wing-root trailing edge, the warp was calculated by linear theory ignoring the cross-coupling between the terms due to the finite wing thickness and due to the loading. In the intermediate triangular region, the warp was faired by taking the lines at constant percentage chord as parabolic arcs. The loading prescribed as a starting point for these calculations consisted of a uniform spanwise distribution of C_L and a triangular chordwise distribution varying linearly from $\Delta C_p = -0{\cdot}27$ at the leading edge to $\Delta C_p = -0{\cdot}03$ at the trailing edge (at the design C_L). The finite-thickness effects that were ignored in the calculations for most of the wing would tend to reduce the loading near the leading and trailing edges and to increase it near the maximum-thickness position.

Typical camber-line shapes at various stations along the span are shown in Fig. 1c. The camber is positive throughout and the maximum value varies from about $0{\cdot}8\%$ at the wing root to rather more than 3% at the tip. One curious point shown in Fig. 1c is that the camber was somewhat less at $0{\cdot}225 \times$ semi-span than at the root station, $0{\cdot}128 \times$ semi-span. This odd feature is a consequence of having adopted different methods for calculating the camber on different parts of the wing.

The spanwise twist distribution is given in Fig. 1d. The wing-body angle is $2{\cdot}9°$ and the total washout across the span amounts to about 6. The actual wing-section shapes in the wing-body junction ($0{\cdot}128 \times$ semi-span) and near the tip at $0{\cdot}95 \times$ semi-span are shown in Fig. 1e. These pictures of the extreme wing sections have been included to illustrate that for this wing designed for $C_L = 0{\cdot}15$, the amount of warp required near the root and tip is by no means excessive.

In discussing the performance achieved by the present design, it should be remembered that there is no actual evidence to show whether the design aims of a uniform spanwise C_L – distribution and triangular chordwise loading were achieved. The pressure-plotting tests on the other model having $4{\cdot}5\%$ thick sections and warped to suit a design C_L of $0{\cdot}25$ showed that in that case, the loading near the wing leading edge was greater than predicted near the root and less near the tip. It is likely that similar discrepancies but to a lesser extent may have existed with the present model and so to achieve in practice the aims quoted above, the camber and twist required near the root and tip could probably be a little less than in the design tested.

These discrepancies between prediction and experiment could be due to various reasons, for example, deficiencies in linear theory and its assumptions, viscous effects or the fact that the calculations were for a wing alone and took no account of the presence of the body. With the actual model, when the wing is at its design C_L, the body will be at a positive incidence and will therefore be inducing some upwash particularly over the wing-root section. One could indeed argue about what is the best choice of wing-body angle. For the present model, the wing was mounted at its estimated zero-lift angle, relative to the body axes. Arguments in favour of this choice are that the lift and drag due to the body and tail unit in the free-flight tests would be the same for both warped- and plane-wing models (provided the lift-curve slope of the wing was not altered by the warp) and secondly, the wing-body angle was kept reasonably small (Figs. 1d, e). On the other hand, it could be argued that a fairer test of the calculations which produce the warped design might have been to set the body at zero incidence when the wing was at its design C_L. This difficulty has been stressed because detailed points such as this could have quite a bearing on the apparent effectiveness of the warp design. It emphasises that there is much more to the problem than simply finding how to design the wing camber and twist for a certain operating C_L.

Also, quite apart from the validity of the methods used to design the camber and twist, there is the overriding question of whether it is right to aim at a constant spanwise C_L – distribution and a triangular chordwise loading. At the time this model was designed, the usual practice was to choose a thickness form and then to calculate the camber and twist to give a certain chordwise loading. More recently, with the attempt to develop better wing-section shapes, the more common approach has been to design for certain upper-surface pressure distribution rather than a certain chordwise loading. These new thoughts on wing-section design have been developed[4] since the present model was designed. The new approach, embodying the more recent work on desirable upper-surface pressure distributions has been used[5] to design the warp for a wing of about the same planform as the present model. This design is to be tested at the National Physical Laboratory. While comparison of these results with those for the present model will be of interest, any differences in performance will not necessarily be related merely to the change in design aims. As mentioned above, a lot of detailed points could result in the design aims not being achieved on either model and so all the results have to be analysed carefully.

The fin-tail unit (Fig. 1a) as noted earlier was not intended to represent an actual aircraft but was merely designed to suit the requirements of the free-flight tests. The tailplane has a planform having good structural properties and an orderly movement of aerodynamic-centre position through the transonic speed range. The tailplane section is RAE 101 and it is 4% thick. The fin section was hexagonal to ease its manufacture.

The description above has been based on the warped-wing model. The shape of the plane-wing model was similar except for the absence of the warp and for the shape of the afterbody. In this case, the afterbody was not parallel but was boattailed as shown in Fig. 13 and instead of the fin-tail unit, a yawmeter comb was mounted as shown in Figs. 13, 14. The relevant points in this layout will be mentioned later when discussing the downwash results in Section 8.

3. *Description of Tests (Warped-Wing Model).*

The tests were made for Mach numbers from $M = 0{\cdot}6$ to $M = 1{\cdot}4$ and for incidences from $-2°$ to $5°$. The drag data obtained at Mach numbers below $M = 0{\cdot}9$ are not included because in absolute terms it was slightly suspect owing to a drift of wind-off zero with temperature.

The tests were made at tunnel stagnation pressure of 1 atmosphere and a temperature varying from 20°C to 45°C according to the Mach number. The test Reynolds number, based on the wing aerodynamic mean chord, varied slightly with Mach number; typical values were:

M	0·7	1·0	1·2	1·4
$R \times 10^{-6}$	3·88	4·37	4·38	4·24

Transition was fixed near the wing, fin and tail leading edges by applying bands of grade 220 carborundum round the leading edge and back to $0{\cdot}05c$ on the wing and $0{\cdot}10c$ on the fin and tailplane. On the fuselage, the roughness band was 1 in. wide and started 1 in. from the nose. A test was made by the azobenzene sublimation technique and this confirmed that the bands were effective in fixing transition at the design C_L (0·15) and the highest Mach number of the test.

The measurements of normal force, axial force and pitching moment were made with an internal strain-gauge balance. Repeatability checks showed that in general, balance zero drifts were small, the only exception being that the drag data for Mach numbers below $M = 0{\cdot}9$ had to be omitted because of significant balance drifts under these conditions. The estimated accuracies are:

$$C_L : \pm 0{\cdot}001$$
$$C_m : \pm 0{\cdot}002$$
$$C_D : \pm 0{\cdot}0002.$$

The quoted values of drag have been corrected to correspond to free-stream static pressure at the base. The actual measured base pressures (Fig. 9) were recorded with a Statham transducer and the errors in drag arising out of inaccuracies in this instrument are completely negligible.

4. *Reduction of Results.*

The lift, drag and pitching moment data were reduced to standard non-dimensional coefficients using a wing area of 3·096 sq. ft, and a wing mean aerodynamic chord of 0·984 ft.

No corrections were applied to the results either for the pitch in the flow in the tunnel or for tunnel interference. The model was set 0·1° nose down and this corresponded to the average angle of pitch in the flow; the variation from this mean value for any given Mach number should be less than ±0·1° and this should have had no material effect on the results of the present test.

The evidence in Ref. 6 suggests that for a model of this size, the tunnel constraint effects on lift should be no more than 2% and also that blockage effects up to say, $M = 0{\cdot}95$ can be treated as negligible. For Mach numbers close to $M = 1{\cdot}00$, the tunnel is effectively too open and it is probable that results obtained for a nominal Mach number of $M = 1{\cdot}00$ would refer to a corrected Mach number of about $M = 0{\cdot}98$. Also, at low supersonic Mach numbers, the flow over the model would be modified by the presence of reflected waves. Ref. 6 shows that the lift and pitching moment for the model without tail would not be seriously affected by the reflected waves but the downwash at the tail could be wrong at some Mach numbers by upwards of about 0·5° and also the measured drag is likely to be too small. The pressure-plotting tests on the similar model to that being considered here, i.e. the one having a 4·5% thick wing of the same planform, have confirmed the conclusions of Ref. 6 that the most serious reflections consist of shock waves which reflect from where the walls intersect a strong expansion field being propagated by the model. Reflections of shock waves such as the bow shock are relatively unimportant. Applying these general conclusions to the present case, means that the drag is likely to be in error until the reflections of the forebody expansion pass

downstream of the wing tip and the downwash may be affected until these reflections are clear of the tailplane. A fairly crude quantitative analysis shows that the drag of the wing-fuselage may therefore be affected between about $M = 0{\cdot}98$ and $M = 1{\cdot}11$ and the downwash and tailplane incremental drag could be affected up to about $M = 1{\cdot}17$. It should be added that these interference effects should not vary greatly with model incidence and so even in this Mach number range, the drag due to lift and $(\partial\epsilon/\partial\alpha)_M$ should still be reasonably reliable.

5. *Drag of Warped Wing-Fuselage Combination.*

The basic drag results for the warped wing-fuselage combination are given in Fig. 2 as curves of C_D against C_L at constant Mach number and in Fig. 3 as curves of C_D against Mach number at constant C_L.

5.1. *Drag at Zero Lift.*

From Fig. 2, it will be seen that at any given Mach number, the drag at zero lift is slightly higher than the minimum drag. This is as would be expected for a warped wing; when the overall C_L is zero, some local parts of the wing would be contributing positive lift and others negative lift so that some vortex drag could be present at $C_L = 0$. Also, it is possible that a localised flow separation may be present near the leading edge on the lower surface; such a separation was observed at zero lift in the pressures measured on the 4·5% thick, $C_L = 0{\cdot}25$ design. These effects result in the measured C_{D0} even at subsonic speeds being slightly greater than the value that would be obtained with a symmetrical wing. Unfortunately, no reliable drag data were obtained with the symmetrical wing and hence an 'effective C_{D0}' has to be derived from the warped-wing data. The minimum C_D usually occurs at about $C_L = 0{\cdot}05$ and in view of this, it was decided to derive an effective C_{D0} from the measured C_D at say, $C_L = 0{\cdot}07$ assuming some appropriate value for K. This calculation is not very sensitive to the actual value assumed for K; for $M = 0{\cdot}9$, for example, for any plausible K, one obtains an effective C_{D0} of 0·0129 as compared with the measured C_{D0} of 0·0132. The distinction between these two values is not very significant when assessing the profile drag at zero lift but it is important when deriving values of K for say, $C_L = 0{\cdot}15$ from the measured data.

Estimates of the profile drag for $M = 0{\cdot}9$ and the appropriate Reynolds number give $C_D = 0{\cdot}0120$ if no allowance is made for the effect of the sweepback of the wing on skin friction or alternatively, 0·0103 if the full allowance[7] is made. The measured effective C_{D0} derived as above was 0·0129 but in arriving at this value, no account has been taken of the possible effect of the roughness bands used to fix transition. Research on other models in the A.R.A. tunnel suggests that the increment in C_D due to these bands could conceivably be as great as 0·0005 and if so, this would reduce the measured value to 0·0124. This figure is in reasonable agreement with the estimate ignoring the effect of sweepback on skin friction but is still 0·0021 above the estimate making the sweep allowance according to Ref. 7. This difference seems to be too great to ascribe to any of the experimental uncertainties and hence the apparent conclusion is that the results do not support the use of this full sweepback factor. The evidence on this point cannot be regarded as conclusive but it is perhaps significant that the results of the tests in Ref. 3 tended to point the same way.

As mentioned earlier, the measured variation of C_D with Mach number between about $M = 0{\cdot}98$ and $M = 1{\cdot}11$ is likely to be affected by tunnel interference and the true flight result at zero lift would probably show a rapid increase in drag close to $M = 1{\cdot}0$ followed by little variation up to at least $M = 1{\cdot}1$. The tunnel results should however give a fair indication of the magnitude of the total increase in C_D over this range of Mach number and it is seen that this amounts to about 0·0021

in C_D. A further increase of about 0·0015 occurs between $M = 1{\cdot}2$ and $M = 1{\cdot}35$. Comparison of the C_D vs. M curves for different values of C_L (Fig. 3) suggests that the start of the supercritical increase in drag, associated with the shock system over most of the wing does not occur until beyond $M = 1{\cdot}35$ at $C_L = 0$ and so it seems fair to deduce that the increase in C_D between $M = 1{\cdot}20$ and $M = 1{\cdot}35$ is probably an indication that the body shape is losing its effectiveness at Mach numbers above the design value of $M = 1{\cdot}17$. However, even at $M = 1{\cdot}35$, $C_L = 0$, the increase in C_D as compared with the value at high subsonic speeds is still only about 0·0035 and this is significantly better than would have been predicted for a 6% thick, 55° swept wing with no body shaping. The value of $\Delta C_D = 0{\cdot}0020$ applying up to $M = 1{\cdot}20$ is remarkably good since even the best of the results achieved with different body shapes in the tests reported in Ref. 3 with a 4·5% thick wing of this planform gave $\Delta C_D = 0{\cdot}0015$. It certainly seems therefore that the body design has been very successful in coping with the requirements at zero lift.

5.2. *Supercritical Drag.*

The start of the main supercritical increase in drag with Mach number at any given C_L due to the appearance of shock waves on the wing, can be deduced from the shape of the C_D vs. M curves in Fig. 3. Similar conclusions can be drawn from the derived values of K plotted in Fig. 4 and discussed in Section 5.3 below.

The supercritical increase in drag appears to occur above about $M = 1{\cdot}35$ at $C_L = 0$, $M = 1{\cdot}25$ at the design $C_L = 0{\cdot}15$, $M = 1{\cdot}20$ at $C_L = 0{\cdot}2$ and $M = 1{\cdot}14$ at $C_L = 0{\cdot}3$.

The first important and encouraging conclusion from these results is that the supercritical increase in drag does not occur until beyond the design conditions of $M = 1{\cdot}2$, $C_L = 0{\cdot}15$. The margins in Mach number at the design C_L and in C_L at the design Mach number are about 0·05. It thus appears that the warp design has been successful in achieving substantial subcritical-type flow under the design conditions with a reasonable margin before any serious ill-effects are likely to occur.

Similar conclusions can be drawn from the flow-visualisation tests on this model. Some representative oil-flow pictures for the wing upper surface are included in Fig. 5*. The middle photograph is for the design conditions of $C_L = 0{\cdot}15$, $M = 1{\cdot}2$. The only shock wave present appears to be a weak shock of very limited extent lying diagonally across the extreme outer wing. The flow over the wing lower surface under the design conditions was also observed but there was no sign of any shock wave or boundary-layer separation.

The photograph on the left in Fig. 5 shows that by $C_L = 0{\cdot}2$ at $M = 1{\cdot}2$, a shock has appeared over the outer half of the span at about $0{\cdot}4c$. As a result, the outflow in the boundary layer over the rear of the wing is substantially greater than at $C_L = 0{\cdot}15$ and close to the tip, the shock appears to be strong enough to be inducing a separation. This sort of flow behaviour was discussed in detail in Ref. 8. An oil-flow pattern was also obtained for $C_L = 0{\cdot}23$, $M = 1{\cdot}2$. The photograph is not clear enough to reproduce in this report but it shows that the shock over the outer third of the semi-span has increased in strength and that the separation now extends over this proportion of the span.

The right-hand photograph in Fig. 5 is for $C_L = 0{\cdot}135$, $M = 1{\cdot}25$. It will be seen that the increase in Mach number from $M = 1{\cdot}20$ has again resulted in the appearance of a weak shock over

* These photographs were taken after shutting down the tunnel. It was however observed on the television screen that no significant distortion of the patterns took place while the tunnel speed was being reduced.

the outer half of the span at about $0{\cdot}4c$ with a suggestion of a vortex forming behind it near the extreme tip. A further picture in this sequence was obtained for $C_L = 0{\cdot}14$, $M = 1{\cdot}30$ and this showed a slight further deterioration near the tip but nothing very dramatic.

Other pictures for $C_L = 0{\cdot}20$ show that the shock wave which was near $0{\cdot}4c$ (Fig. 5) at this C_L at $M = 1{\cdot}20$ moves forward to near $0{\cdot}3c$ at $M = 1{\cdot}30$ and is then much more clearly defined with undoubtedly a separation vortex behind the shock front. The vortex lies farther in along the wing than at $M = 1{\cdot}20$; its centreline appears to cross the wing trailing edge at about $0{\cdot}85 \times$ semi-span and the secondary separation line farther outboard can also be seen.

Summing up the correlation between the flow pictures and the drag data, it seems that the start of the relatively rapid increase in drag with Mach number roughly corresponds with when the shock over the outer wing is strong enough to induce a separation and a vortex. A weak shock wave can be present before this. Particularly at the higher values of C_L, this weak shock can increase considerably the spanwise drift in the boundary layer over the rear of the wing. This increased boundary-layer drift at the higher values of C_L could be the main reason why the increase in C_D between say, $M = 0{\cdot}97$ and $M = 1{\cdot}2$ amounts to about $0{\cdot}0034$ at $C_L = 0{\cdot}2$ as compared with only $0{\cdot}0021$ at $C_L = 0$.

Broadly speaking, therefore, it would seem that the warp design has been successful in its main aims and that an even better drag performance would have been obtained if it were not for the boundary-layer effects over the rear of the wing upper surface. The importance of these boundary-layer effects has been confirmed by the fact that the results of the tests on this model in the 8 ft Tunnel at the Royal Aircraft Establishment, Bedford, have shown that the variation of C_D with C_L particularly at the higher values of C_L and Mach number is sensitive to a change in Reynolds number between 1×10^6 and 4×10^6, being greater at the lower Reynolds number.

5.3. *Drag Due to Lift.*

To assess the performance of the wing-fuselage configuration in relation to theoretical predictions and in terms of the parameters used in project analyses, it is useful to derive values of K, the drag-due-to-lift factor. A comparison between values derived from the measured drag data and those predicted theoretically is presented in Fig. 4.

Before discussing these results in detail, it is necessary to explain the method used for deriving values of K from the experimental data. It is now generally accepted that to assess the effectiveness of a camber or warp design, one should think in terms of values of K defined by the equation:

$$C_D = C_{D0\,s} + \frac{K}{\pi A} C_L^2$$

where the suffix s refers to the corresponding plane, symmetrical wing. The values of K so defined can be compared directly with the values for the corresponding plane wing and there is no need to introduce any other quantities in order to judge the improvement achieved with the warp. Any other definition such as

$$C_D = C_{D0} + \frac{K}{\pi A} C_L^2$$

or

$$C_D = C_{D\,\min} + \frac{K}{\pi A} (C_L - C_{L\,\mathrm{opt}})^2$$

where

$$C_{D\,\min} \text{ occurs at } C_{L\,\mathrm{opt}},$$

would have the weakness that when comparing results for the plane and warped wings, one would have to consider changes in both K and C_{D0} or $C_{D\,\min}$ and it would not immediately be obvious which change was the more important.

Use of $C_{D0\,s}$ in deriving K makes it easier therefore to appreciate the significance of the derived values of K, but on the other hand it increases the difficulties in getting a reliable answer from experimental tests. For example, even for cases where drag data have been obtained for both warped wing and the corresponding plane wing, the accuracy of the derived values of K, particularly at low C_L, now depends vitally on whether the absolute values of C_D obtained for the two models are relatively correct. In the present case, it is even more difficult because no reliable drag measurements were obtained from the A.R.A. tests on the plane-wing model and so $C_{D0\,s}$ has to be derived from the warped-wing results. As described earlier, an effective $C_{D0\,s}{}'$ was derived from the measured C_D values for $C_L = 0{\cdot}07$:

$$C_{D0\,s}{}' = (C_D)_{C_L=0{\cdot}07} - \frac{K}{\pi A}(0{\cdot}07)^2. \tag{1}$$

Initially, the theoretical values of K (as per the dashed curve in Fig. 4), were fed into this equation. Values of K for the warped wing were then obtained from

$$C_D = C_{D0\,s}{}' + \frac{K}{\pi A} C_L{}^2 \tag{2}$$

for $C_L = 0{\cdot}15$, $0{\cdot}20$, $0{\cdot}25$ and $0{\cdot}30$. It will be seen (Fig. 4) that the variation of K with M for $C_L = 0{\cdot}15$ is fairly smooth up to about $M = 1{\cdot}25$ and that then, a rapid increase in K occurs corresponding with the appearance of a strong shock wave on the wing upper surface. This would probably not happen until a higher Mach number at lower values of C_L and so for $C_L = 0{\cdot}07$, the smooth variation of K with M should be maintained up to nearer $M = 1{\cdot}4$. A check was then made that using this variation of K with M rather than the theoretical variation in deriving values of $C_{D0\,s}{}'$ by equation (1) above did not materially affect the values of K deduced by equation (2). It was found that small changes had to be made at $C_L = 0{\cdot}15$ but the effect was quite negligible at the higher values of C_L. The values of K plotted in Fig. 4 for $C_L = 0{\cdot}15$, $0{\cdot}20$, $0{\cdot}25$ and $0{\cdot}30$ are obtained at the end of this iterative process.

It will be realised from the above that the derivation of appropriate values of K for the warped wing is not easy and it obviously depends critically on whether the right values have been deduced for $C_{D0\,s}{}'$. The method described above was based on the assumption that at $C_L = 0{\cdot}07$ for the present wing, the warp was not giving any increase in the vortex or profile drags. While it is thought that this is reasonable in the present case, a method of this sort would clearly not be satisfactory for a more highly warped design. Hence this effective $C_{D0\,s}{}'$ is either equal to or greater than the value of C_{D0} for the symmetrical plane wing and if the derived values of K are in error, they will tend to be lower than the true values. To illustrate this point in quantitative terms, one can consider the values of K for the design conditions of $C_L = 0{\cdot}15$, $M = 1{\cdot}2$. According to Fig. 4, the value is $1{\cdot}55$ but if $C_{D0\,s}{}'$ were wrong by merely $0{\cdot}0002$, the value would have been $1{\cdot}70$. Even the measured values of C_D for the warped wing are not necessarily accurate to better than $\pm 0{\cdot}0002$ in C_D and obviously, the derived values of $C_{D0\,s}{}'$ cannot be any better than this. Hence, basically, the values of K for $C_L = 0{\cdot}15$ could be in error by $\pm 0{\cdot}15$; at higher values of C_L, the uncertainty rapidly decreases. These figures may have over emphasised the difficulty of the problem. One can also judge the accuracy of the derived values of K by considering whether the trends appear plausible or not.

In actual fact, the variation of K with Mach number at $C_L = 0{\cdot}15$ and with C_L at $M = 1{\cdot}2$, as shown in Fig. 4, appears quite reasonable. In both cases, increases in K correlate with when, as described earlier, the oil-flow patterns are indicating the appearance of a strong shock and consequent flow separation. If the assumed values of C_{D0_s}' had been in error by more than about $0{\cdot}0003$ the graph showing the variation of K with M and C_L would have appeared completely implausible: for example, a reduction in K would have been obtained at $M = 1{\cdot}2$ with increasing C_L from $0{\cdot}15$ to $0{\cdot}20$ and this would have been completely at variance with the evidence of the oil-flow patterns.

To sum up the discussion above, one can therefore say that it is extremely difficult to derive reliable values of K, particularly for $C_L \leqslant 0{\cdot}15$ but nevertheless the trends shown by the values in Fig. 4 appear quite plausible and therefore it seems fair to place some confidence in these derived values. Any comparison between the measured and theoretical values should not be interpreted too literally and one should not argue about small differences but, nevertheless, it seems possible to draw certain definite conclusions:

(1) at subsonic speeds, K is about $1{\cdot}2$ up to $C_L = 0{\cdot}2$ rising to about $1{\cdot}3$ at $C_L = 0{\cdot}3$. These values compare with a theoretical prediction[9] for the vortex drag-due-to-lift factor, K_V, of $1{\cdot}078$;

(2) at the design conditions, $M = 1{\cdot}2$, $C_L = 0{\cdot}15$, the value derived from the experimental results is $K = 1{\cdot}55$. This compares with theoretical predictions of either $1{\cdot}28$ or $1{\cdot}33$ according to whether the wave drag-due-to-lift factor, K_W, is taken as the Jones lower-bound value or is obtained by interpolation from the charts in Ref. 9. The values from Ref. 9 should apply in the present case provided the warp is achieving the design aims of constant C_L across the span and triangular chordwise loading;

(3) if it is assumed that the vortex drag factor is independent of Mach number, the above value of $K = 1{\cdot}55$ if interpreted literally would correspond to $K_V = 1{\cdot}13$, $K_W = 2{\cdot}1$. If, on the other hand, K_V were taken as $1{\cdot}20$ one would obtain $K_W = 1{\cdot}75$. This demonstrates that K_W is even more difficult to determine from experimental data than K itself. There is however a much more fundamental point than just the question of accuracy. From what was said in Section 5.2, it is quite likely that the increase in K for $C_L = 0{\cdot}15$ between $M = 0{\cdot}9$ and $M = 1{\cdot}2$ could be related to an increase with Mach number in the spanwise boundary-layer drift over the rear of the wing upper surface, thus decreasing the lift contribution from the rear and so distorting the chordwise loading. Pressure-plotting tests on various other 55° sweptback wings at A.R.A. have confirmed that increasing Mach number in this range can have this sort of effect. If this is the right explanation for the increase in K with Mach number, it is quite wrong to assume that K_V is independent of Mach number and one could just as well analyse the value of $K = 1{\cdot}55$ as indicating that $K_W = 1{\cdot}0$ and that K_V has increased from about $1{\cdot}15/1{\cdot}2$ at subsonic speeds to $1{\cdot}35$ at $M = 1{\cdot}2$. Probably the right interpretation lies somewhere between these two extremes but this illustrates the difficulty in analysing experimental results in terms of the concepts of K_V and K_W particularly when no pressure-plotting data are available to indicate the physical reasons for the changes with Mach number;

(4) at higher values of C_L, even before a strong shock wave is present, the increase of K with Mach number above $M = 1{\cdot}0$ becomes more rapid. The earlier discussion has suggested

that this could be at least partly due to an increase in the viscous boundary-layer effects and extrapolating the trends evident in the 8 ft tunnel results over the range from $R = 1 \times 10^6$ to $R = 4 \times 10^6$, it is likely that these values of K at the higher C_L might be reduced at flight Reynolds numbers.

Although the derived values of K are higher than the theoretical estimates, it still remains true that they are better than might have been expected from the general mass of data for wings with highly swept planforms. This again suggests that the warp design is being reasonably successful. In the early calculations in Ref. 1, Bagley suggested that the value of K for a wing of this planform in viscous flow would be about 1·65 but this value was based on an analysis of experimental results at low speed and if it were increased to allow for K_W estimated according to the Jones lower-bound variation, this would have given $K = 1{\cdot}85$ at $M = 1{\cdot}2$. This compares with $K = 1{\cdot}55$ from the experimental results and even allowing for the uncertainties discussed earlier, the experimental results would seem to be better than the original estimates.

5.4. *Lift/Drag Ratios.*

The variation of L/D with C_L for $M = 0{\cdot}9$, $1{\cdot}10$, $1{\cdot}2$, $1{\cdot}3$ and $1{\cdot}4$ is given in Fig. 6a and the variation of $(L/D)_{\max}$ and L/D for $C_L = 0{\cdot}15$ with Mach number is given in Fig. 6b. The variation in L/D between $M = 0{\cdot}98$ and $M = 1{\cdot}1$ is not shown in Fig. 6b or in any other similar figures because this is the Mach number range where the results are subject to significant tunnel interference. Corresponding values of L/D have also been deduced for a typical full-scale configuration with a body length of 200 ft, a wing mean chord of 35 ft, flying at an altitude of 40,000 ft (this gives a Reynolds number, based on the wing chord, of about 80×10^6). The values for the full-scale configuration have been derived from the tunnel results by making a correction for the reduction in skin-friction drag due to the difference in Reynolds number. In view of the conclusion of Section 5.1, this change in skin-friction drag was estimated making no allowance for wing sweepback. If the full sweep factor[6] had been included, the resulting values of L/D would have been about 0·5 lower than those shown in Fig. 6b.

It must be stressed that the analysis of the drag results in terms of the C_D vs. M curves, values of K etc., as discussed in the preceding sections, is the soundest method of assessing the performance of the warped wing-fuselage design. One must not jump to quick conclusions by looking at the values of L/D and quoting them out of context. They are critically dependent not only on the effectiveness of the wing warp, wing-body junction shape etc., but also on the shape of the forebody, the fact that the afterbody is parallel and not boattailed, the position of the wing on the body and so on. Also, they are values for a wing-fuselage combination; corresponding values for a complete aircraft would be lower because of the drag of the fin-tail unit, engine nacelles etc., but the question of how much lower would depend on the skill with which these extra components were added to the design. For example, by careful shaping of the afterbody, it might be possible to add the fin-tail unit with only a small reduction in the overall L/D but as will be seen in Section 6 below, the addition of the particular fin-tail unit to be used in the free-flight trials reduced L/D by as much as 2·8 at the design Mach number and C_L. These arguments can also be supported by the results of some comparative tests made with the 4·5% thick, $C_{L\,\text{des}} = 0{\cdot}25$ wind-tunnel model with alternatively a parallel and a boattailed afterbody: differences in L/D of between 0·5 and 1·0 were observed at supersonic speeds.

Despite these reservations, various interesting conclusions can be drawn from Fig. 6b. It will be seen that the values of $(L/D)_{max}$ for the assumed flight case vary from about 16·5 at subsonic speeds to about 14 at $M = 1·1$, 13 at $M = 1·2$ and 9·7 at $M = 1·4$. Values of C_L corresponding to $(L/D)_{max}$ vary from $C_L = 0·24$ at $M = 0·9$ to about $C_L = 0·20$ at $M = 1·2$ and above. It was pointed out in Ref. 10 that engine and weight considerations would probably result in the optimum range being obtained by flying at a C_L—value of the order of 0·7 times that for $(L/D)_{max}$. Hence it seems appropriate to consider the values of L/D for $C_L = 0·15$, the design C_L of the warp rather than $(L/D)_{max}$. These values of L/D for $C_L = 0·15$ tend to be about 8% lower than the values of $(L/D)_{max}$; this compares with a figure of about 6% assumed by Dr. Küchemann in his review in Ref. 10.

The actual value of L/D for $C_L = 0·15$, $M = 1·2$ is about 12·0 and this value is substantially maintained up to about $M = 1·25$. By $M = 1·4$ it has fallen to about 9·0, but this implies only about a 12% reduction in range. A value of 12 for $M = 1·2$ is the sort of value that has been suggested for an economic aircraft design cruising at this Mach number. Since this value has here been obtained for only the simple wing-fuselage with no fin-tail unit, it seems that the present design is not quite good enough but this in itself is not discouraging. In his original note[1], Bagley suggested that a thickness/chord ratio of 4·5% (with a cruise C_L of probably about 0·25) rather than 6% would be needed for a 55° sweptback wing at $M = 1·2$. With refinements in wing-section design[4] and warp distributions[6], it may not now be necessary to reduce the wing thickness/chord ratio to 4·5%.

On the other hand, the value of 9 obtained for L/D at $C_L = 0·15$, $M = 1·4$ is already higher than what has been thought possible with a 55° sweptback-wing layout. Clearly if one had tested a configuration designed for flight at $M = 1·4$ rather than $M = 1·2$, even better values of L/D would probably have been obtained. Hence the reduction in cruise L/D with increase in design Mach number should not be nearly as catastrophic as suggested in some references.

6. *Incremental Drag of Fin-Tail Unit.*

The increments, $\Delta C_{D\,FT}$, in C_D due to the fin-tail unit used in the free-flight tests are presented in Figs. 7a, b, c for tail settings of $-6°30'$, $-2°49'$ and $0°52'$. These values have been derived in a form suitable for use in analysing the results of the free-flight tests. The values of C_D for a given Mach number obtained in the tunnel tests for the model with and without the fin-tail unit were subtracted at a *constant model incidence* and *not* at a constant model C_L and the variation of $\Delta C_{D\,FT}$ with Mach number at constant values of C_L as plotted in Fig. 7 was produced by cross-plotting. The quoted values of C_L refer to the full configuration with tail and so the data can be used directly as a correction to the free-flight results.

It will be seen that the values of $\Delta C_{D\,FT}$ reach a maximum, as would be expected from area-rule considerations, at a Mach number near $M = 1·0$. Above about $M = 1·14$, there is a steady decrease in $\Delta C_{D\,FT}$ with increasing Mach number. The values at these higher Mach numbers depend quite significantly on both C_L and tail setting and these points should be taken into account when analysing the free-flight results. Once again, the values for Mach numbers in the range from $M = 0·98$ upwards may be subject to significant tunnel interference. For example, the maximum values of $\Delta C_{D\,FT}$ occur near nominal Mach number of $M = 1·02$, but on the evidence in Ref. 5 this would probably correspond to a corrected Mach number of $M = 1·00$. Also, the relatively strong shock reflection of the forebody expansion field may not clear the tailplane until near $M = 1·17$ and so

the values of $\Delta C_{D\,\mathrm{FT}}$ may be in error up to near $M = 1{\cdot}2$ whereas one has some confidence in saying that the values of C_D for the wing-fuselage combination should be fairly reliable beyond about $M = 1{\cdot}1$. Comparison of the results of the free-flight and tunnel tests in the Mach number range between $1{\cdot}0$ and $1{\cdot}2$ will therefore be of particular interest in helping to show how serious are the tunnel interference effects in this range.

There is however another possible source of discrepancy between the results from the tunnel and free-flight tests. In the tunnel tests the base pressure, particularly at supersonic speeds, was found to be very sensitive to the presence of the tail and to the tail setting. This is shown by the results plotted in Fig. 8. At supersonic speeds, this base-pressure correction could change the drag increment due to the fin-tail unit by as much as $0{\cdot}0035$ in C_D. In the free-flight tests, it seems likely that tail setting will affect the pressures over the rear tapering fuselage (Fig. 1) in a similar qualitative fashion to its effect on the base pressures in the tunnel test. In quantitative terms, however, the effects may not be the same and hence, strictly speaking, correcting the tunnel results to correspond to free-stream static pressure at the base may not be giving the most appropriate tailplane incremental drags to apply to the free-flight data.

Fig. 9 has been prepared to show how critically the drag data to be obtained in the free-flight tests are likely to depend on the drag of the fin-tail unit. Fig. 9 gives the variation of L/D with Mach number for $C_L = 0{\cdot}15$. Curve A gives the values obtained from the tunnel tests for the wing-fuselage and curve C gives the values for the complete model ($\eta_T = -2°49'$). Curve D indicates the correction to curve C having converted to the Reynolds number of the free-flight tests ($R \simeq 10 \times 10^6$). Curve B is taken from Fig. 6b and gives the values for the wing-fuselage converted to a typical full-scale Reynolds number. If the wave drags obtained in the tunnel and free-flight tests were the same, this figure would mean that curve D would be the answer obtained in the free-flight tests whereas B would be the answer deduced from the free-flight tests for the wing-fuselage configuration, full scale. Hence, for example, for $M = 1{\cdot}2$, the value of L/D obtained in the free-flight tests on this assumption would be $6{\cdot}4$ and subtracting the drag of the fin-tail unit, this would become $9{\cdot}2$ and converting to full-scale Reynolds number, it would become $12{\cdot}0$. It is not the precise values that are the point here; it is the fact that the L/D for the wing-fuselage full scale is almost twice the value that would actually be measured in the free-flight tests. This emphasises the vital nature of these corrections for this type of configuration designed to have little wing wave drag at supersonic speeds.

7. *Lift and Pitching-Moment Characteristics.*

C_L vs. α curves for various Mach numbers are given in Figs. 10a, b and the variation of $(\partial C_L/\partial\alpha)_M$ with Mach number is given in Fig. 11. C_m vs. C_L curves for the model without tail and for the complete model with different tail settings are given for all the test Mach numbers in Figs. 12a to n and the derived variation of aerodynamic-centre position with Mach number is given in Fig. 11.

These results call for little comment except for the general point that within the C_L range of these tests, i.e. up to about $C_L = 0{\cdot}3$, no very serious effects are apparent.

The C_L vs. α curves are, in general, reasonably linear. Poorer slopes are observed both below $C_L = 0{\cdot}1$ at subsonic speeds and also at the highest C_L and Mach numbers. The reduction occurs above about $C_L = 0{\cdot}25$ at $M = 1{\cdot}3$ and $C_L = 0{\cdot}16$ at $M = 1{\cdot}4$. These values presumably correspond to when the loss in lift due to the shock-induced separation exceeds any increase in lift due to the vortex associated with this separation. The loss in lift could result from a forward

movement of the shock due to the effects of the separation. Figs. 12m, n show that a pitch-up tendency occurs soon afterwards.

It is particularly important to note that the first break in the C_M vs. C_L curves occurs in a nose-down rather than a nose-up sense. This change could correspond either with the development of local supersonic flow ahead of the shock or to the appearance of a vortex associated with the shock-induced separation, but with no pressure-plotting data and with only a few oil-flow pictures there is insufficient evidence to determine this. It is clear however that these nose-down changes are occurring well beyond the design C_L, M condition. For example, at $M = 1{\cdot}19$, the first break (nose-down) in the pitching-moment curves is not observed until near $C_L = 0{\cdot}27$, i.e. $0{\cdot}12$ above the design C_L, while with increase in Mach number at the design C_L, the first break is not evident until $M = 1{\cdot}3$, i.e. $0{\cdot}1$ in Mach number above the design value. These margins are considerably greater than those for the onset of a significant drag-rise; the margins for a nose-up break would be even greater.

The aerodynamic centre at the design $C_L = 0{\cdot}15$ varies little with Mach number up to $M = 0{\cdot}94$, beyond which there is a steady rearward movement of about $0{\cdot}09\bar{c}$ by $M = 1{\cdot}19$ or $0{\cdot}18\bar{c}$ by $M = 1{\cdot}4$. As would be expected, therefore, for wings designed to have subcritical-type flow at $M = 1{\cdot}2$, only part of the 'transonic' shift in aerodynamic centre has occurred by this Mach number. This point should be remembered when estimating possible trim drag penalties. For this particular configuration, at least half the shift occurs at Mach numbers beyond the design value. Finally, C_{m0} due to the wing warp is seen to be small, being about $0{\cdot}005$ throughout the test Mach number range.

8. *Downwash: Comparison of Results for Warped and Plane Wings.*

The downwash results for both plane- and warped-wing models are shown in Fig. 15 in the form of ϵ vs. M for $\alpha = 0$ and $(\partial\epsilon/\partial\alpha)_M$ vs. M, mean values being taken over the range of C_L from 0 to $0{\cdot}2$. As explained earlier, the results for the plane wing were obtained from the yawmeter comb shown in Fig. 14 mounted in place of the tailplane. Comments regarding the accuracy of these measurements are contained in the Appendix. Although the comb consisted of 5 yawmeter heads giving a coverage over the tailplane span, little spanwise variation was observed except at the outermost position and it was therefore thought sufficient to present in this report results for a single yawmeter only.* The downwash results for the warped-wing model were of course obtained from an analysis of the C_m vs. C_L curves contained in Figs. 12a to n.

Interpretation of these downwash results is complicated by tunnel interference effects which could be present from about $M = 0{\cdot}98$ to near $M = 1{\cdot}2$. The most serious effects are probably those due to the shocks being reflected from where the tunnel walls intersect the forebody expansion field. These are likely to be in the region of the tailplane position in the Mach number range from about $M = 1{\cdot}1$ to $M = 1{\cdot}17$. Any reflections of the body bow shock would not have cleared the tailplane until $M = 1{\cdot}27$ but these reflections should be considerably alleviated by the perforated walls. It should perhaps be explained that although ideally, for the perfectly symmetrical case, reflections from opposite walls should have cancelled as regards changes in flow inclination, the model is mounted 6 in. above the tunnel centreline and the tailplane itself is a further 8 in. above the model centreline. The model incidence will introduce further asymmetries. Ref. 5 shows that these tunnel interference effects can cause apparent changes in downwash amounting to about $0{\cdot}5°$.

* All the values were however considered when planning the free-flight trials.

Fig. 15 shows that the variation of $(\partial\epsilon/\partial\alpha)_M$ with Mach number is basically similar for the two models, the values being slightly less for the plane wing. This difference is to be expected since the spanwise loading would be changed by the wing warp. At low values of C_L, the wing warp should have increased the loading near the wing root and reduced it near the tip; this should have increased the values of $(\partial\epsilon/\partial\alpha)_M$ at the tailplane and this is consistent with the experimental results. As regards the variation of ϵ with Mach number, also shown on Fig. 15, a discontinuity in the results for the plane wing was only to be expected in the range $M = 1{\cdot}10$ to $M = 1{\cdot}15$ since the flow disturbance originating from near the base of the model (Fig. 13) should be crossing the yawmeters in this Mach number range. It is therefore reasonable to fair over this discontinuity. Over most of the test Mach number range, therefore, the downwash at $\alpha = 0°$ is about $0{\cdot}5°$ higher for the warped-wing model and a qualitative change in this direction could once again have been predicted from consideration of the effects of the wing warp on the spanwise loading.

9. *Conclusions.*

The results for the warped-wing model can be considered as encouraging. The flow pictures confirm that over most of the wing, subcritical-type flow is being maintained under the design conditions of $M = 1{\cdot}2$, $C_L = 0{\cdot}15$. It appears that the supercritical increase in drag does not occur until beyond this condition. The margins in Mach number at the design C_L and in C_L at the design Mach number before the start of the serious supercritical increase in drag or the appearance of a shock-induced separation seem to be of the order of $0{\cdot}05$. The corresponding margins before any significant changes in pitching moment occur are about twice this and even then, the first changes are in a nose-down sense.

It is difficult to derive precise values of K but it seems that at subsonic speeds and low C_L, K is near $1{\cdot}2$ as compared with a theoretical prediction for K_V of $1{\cdot}08$. At the design conditions, $M = 1{\cdot}2$, $C_L = 0{\cdot}15$, the approximate value from the experimental results is $K = 1{\cdot}55$ as compared with a theoretical prediction of $1{\cdot}33$. There is some reason for believing that the excess K observed in experimental results under these conditions and more particularly, the increase which occurs at higher C_L are to a considerable extent due to viscous effects and could be interpreted as an increase of K_V with Mach number. It may be less at higher Reynolds numbers. Even so, the values of K observed in these tests at about $R = 4 \times 10^6$ are better than would have been predicted on the basis of the results for other wings. This is again encouraging evidence of the possibilities of wing warp for this sort of design C_L and planform.

Analysis of the values of C_D obtained at zero lift provides no evidence in favour of the existence of a sizeable sweep factor on skin-friction drag.

For the simple wing-fuselage at full-scale Reynolds number, L/D for $C_L = 0{\cdot}15$ varied from about 12 at $M = 1{\cdot}2/1{\cdot}25$ to about 9 at $M = 1{\cdot}4$.

The incremental drag due to the fin-tail unit used in the free-flight tests can reduce the lift/drag ratio for $C_L = 0{\cdot}15$ by almost $3{\cdot}0$ at $M = 1{\cdot}2$ and it seems that the values of L/D that would be obtained in free flight for the complete configuration may be only about half of the values for the wing-fuselage at full-scale Reynolds numbers.

Only about half the transonic shift in aerodynamic centre has occurred by $M = 1{\cdot}2$. The downwash results also show that the maximum $(\partial\epsilon/\partial\alpha)_M$ occurs beyond $M = 1{\cdot}0$ rather than subsonically as would be the case with a less swept wing.

REFERENCES

No.	*Author(s)*	*Title, etc.*
1	J. A. Bagley	An aerodynamic outline of a transonic transport aeroplane. A.R.C. 19 205. October, 1956.
2	G. G. Brebner	A design of swept wing planforms to improve tip-stalling characteristics. A.R.C. 17 264. July, 1954.
3	A. B. Haines, T. E. B. Bateman and K. Rollins	Tests in the A.R.A. Transonic tunnel on a series of swept wing-body models with different body shapes. A.R.A. Wind Tunnel Note 26. May, 1959.
4	H. H. Pearcey	The aerodynamic design of section shapes for swept wings. Paper presented at the Second International Congress, Zürich. September, 1960.
5	R. C. Lock and E. W. E. Rogers	Aerodynamic design of swept wings and bodies for transonic speeds. Paper presented at the Second International Congress, Zürich. September, 1960.
6	F. O'Hara, L. C. Squire and A. B. Haines	An investigation of interference effects on similar models of different size in various transonic tunnels in the U.K. A.R.A. Wind Tunnel Note 27. A.R.C. 21 094. February, 1959.
7	J. Weber and G. G. Brebner ..	A simple estimate of the profile drag of swept wings. A.R.C. 15 246. October, 1952.
8	F. O'Hara and J. B. Scott-Wilson	An investigation of the flow over a half-wing model with 60·5 degree leading edge sweepback, at a high subsonic and supersonic speeds. A.R.C. C.P. 471. November, 1955.
9	J. A. Bagley and J. A. Beasley ..	The shapes and lift-dependent drags of some swept-back wings designed for $M_0 = 1 \cdot 2$. A.R.C. C.P. 512. June, 1959.
10	D. Küchemann	Some considerations of aircraft shapes and their aerodynamics for flight at supersonic speeds. A.R.C. 21 102. June, 1959.
11	G. M. Roper	Formula for calculating the camber surfaces of thin swept-back wings of arbitrary plan-form with subsonic leading edges, and specified load distribution. A.R.C. R. & M. 3217. June, 1959.

APPENDIX

Accuracy of Measurement of Flow Direction (Plane-Wing Tests)

The yawmeter heads were calibrated, in the pitch plane only, by R.A.E., Bedford. Of the five heads used, only one was calibrated through the full test range of Mach number. The remaining four were only calibrated at $M = 1{\cdot}4$ and certain higher Mach numbers outside the A.R.A. test range. The variation of calibration factor with Mach number was significant, viz., $d(\Delta p/H)/de$ varying from $0{\cdot}0093$ at $M = 0{\cdot}72$ (for the first yawmeter) to $0{\cdot}0163$ at $M = 1{\cdot}4$. It was assumed that the other yawmeters possessed a similar variation, i.e. the ratio of their respective factors to that for the first yawmeter was assumed to be independent of Mach number. The limited information available indicated such a trend. Any estimate of accuracy should however bear this sweeping assumption in mind. Another source of inaccuracy will be in the measurement of the pressure difference across the holes during the test. For all the conditions except those at the highest model incidences, this pressure difference was measured on an alcohol manometer; when the range of the alcohol manometer was exceeded, the pressures were switched on to mercury manometers. The manometer readings were recorded photographically.

The maximum observer error of $0{\cdot}1$ in. alcohol is equivalent to about $0{\cdot}05°$ in flow direction. However, owing to the small diameter of the yawmeter holes and the length of pressure tubing, the pressure lag of the system was significant and caused a maximum repeatability error of $0{\cdot}15°$, the average being about $0{\cdot}05°$, and this figure is thought reasonably representative of the accuracy of flow angularity measurement at the yawmeter head using given calibration data. This experimental error means that the derived values of $\partial\epsilon/\partial\alpha$ are accurate to within about $\pm 0{\cdot}02$.

An attempt was made to obtain the absolute value of ϵ by carrying out similar tests at zero model incidence with the yawmeter heads set both normal and rotated 180° about their longitudinal axes. This gave apparent values of downwash of $0{\cdot}5°$ to $0{\cdot}6°$ at subsonic speeds changing at about $M = 1{\cdot}15$ to an upwash of equal magnitude. The change of apparent downwash at about $M = 1{\cdot}15$ coincided with the passage of the flow disturbance from the fuselage base over the yawmeter heads. As would be expected, the variation of 'instrument error', i.e. the error in yawmeter reading attributable to instrument asymmetries, etc., undergoes little change over the whole Mach number range except at about $M = 1{\cdot}15$ when the fuselage base disturbances tend to cause a spuriously high value.

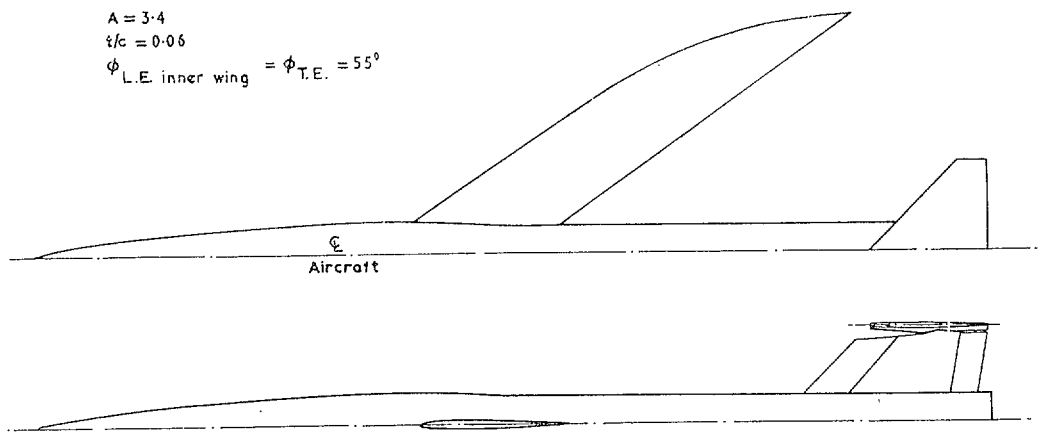

FIG. 1a. Half general arrangement of warped-wing model (scale: 1/16th model size).

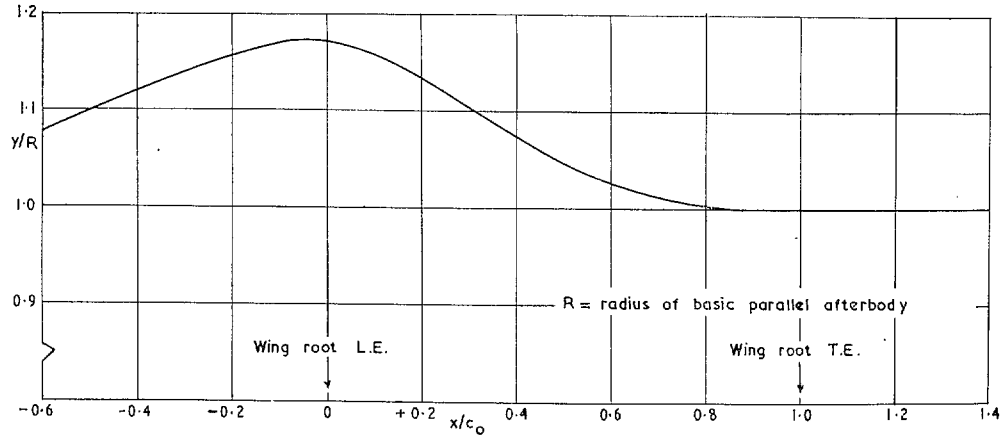

FIG. 1b. Wing-body junction shape, designed by area rule for $M = 1·2$.

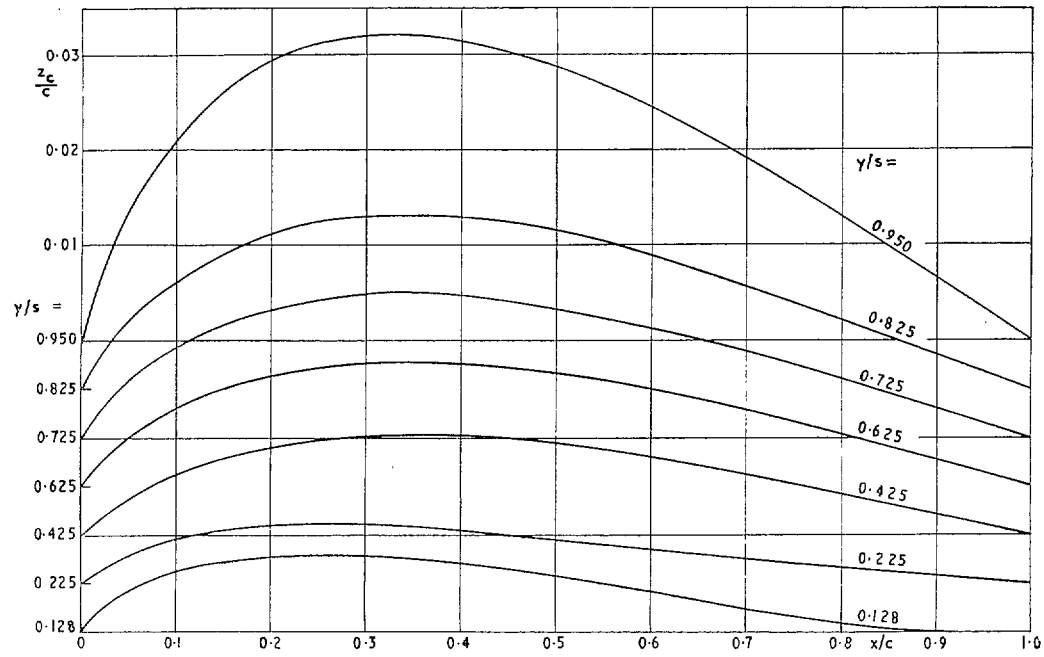

FIG. 1c. Camber lines at various positions along span.

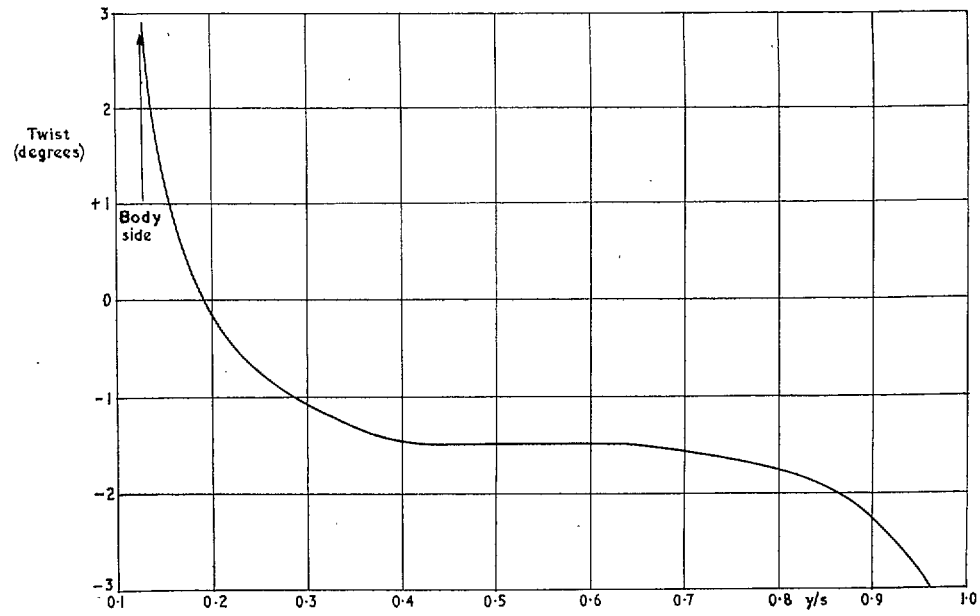

FIG. 1d. Spanwise twist distribution.

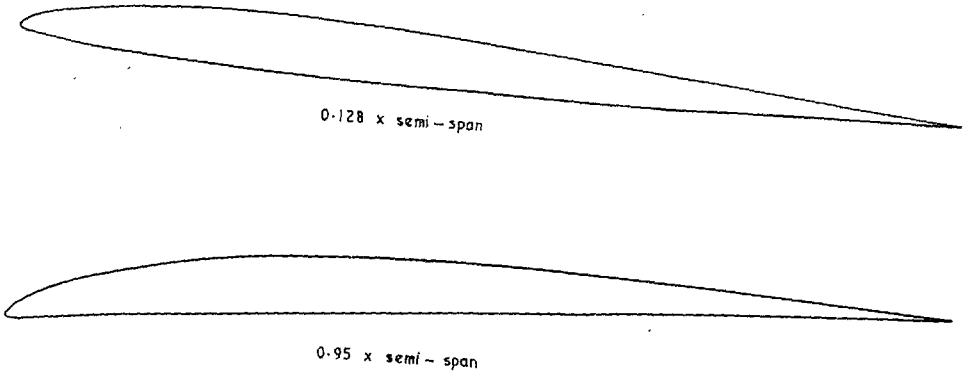

FIG. 1e. Wing sections near root and tip.

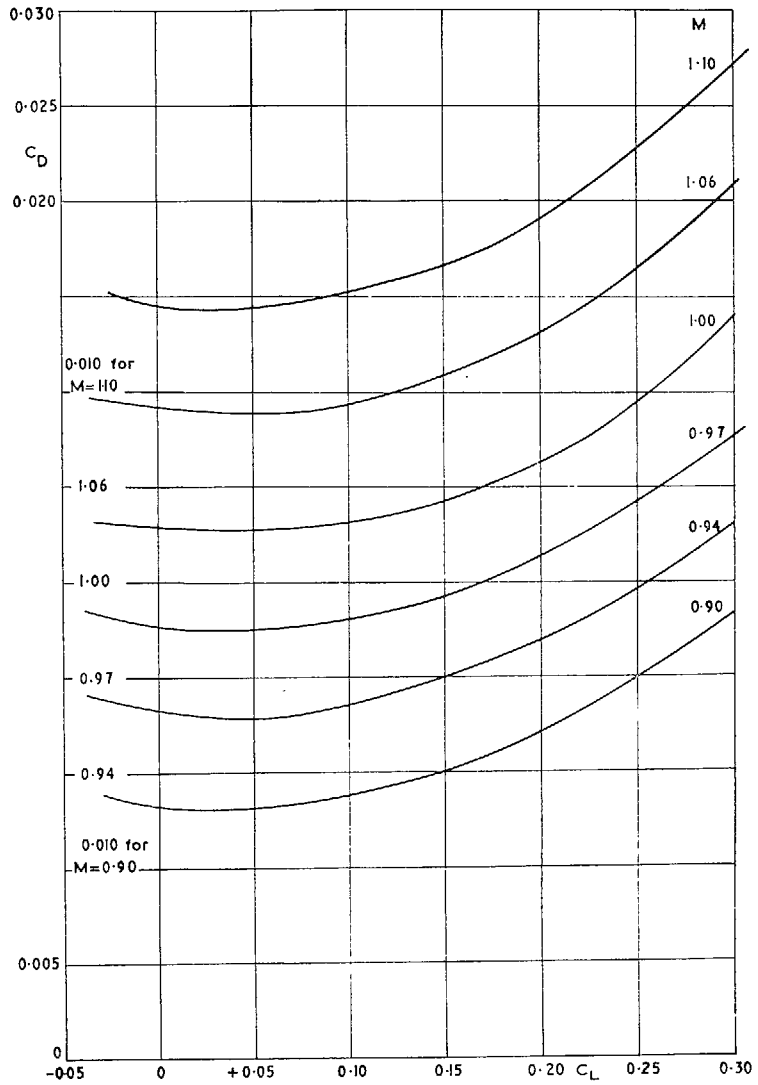

(a)

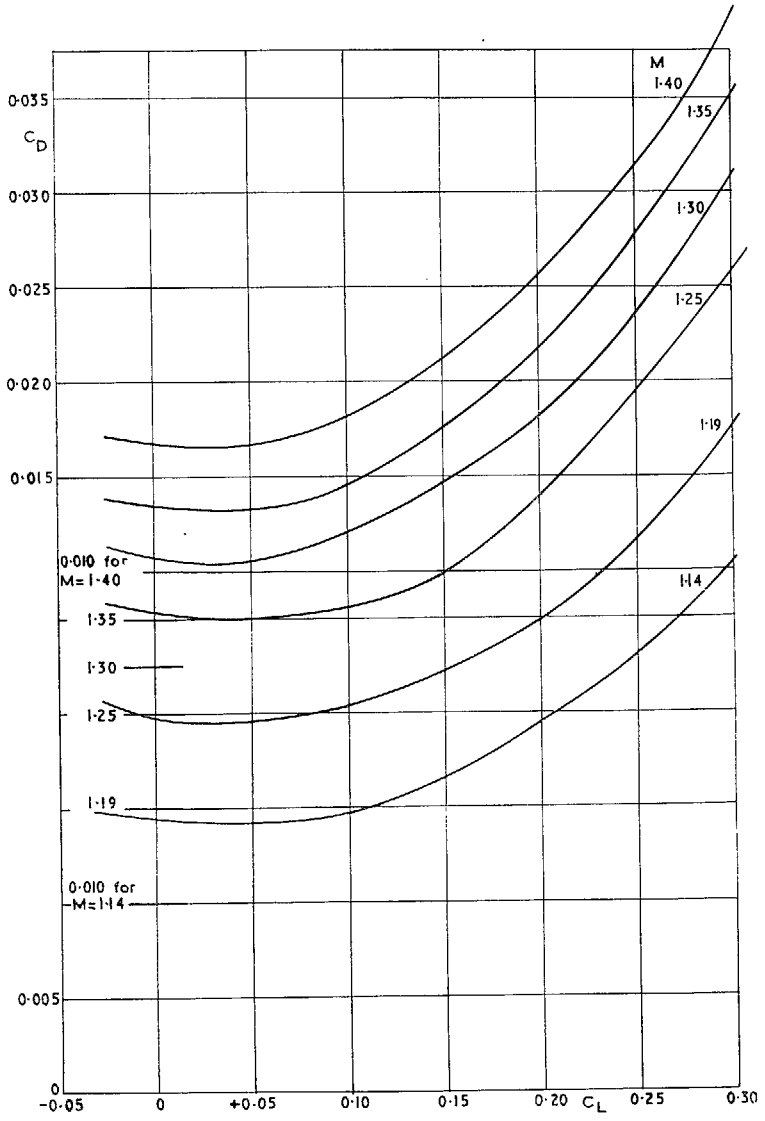

(b)

FIG. 2. Variation of C_D with C_L: model without fin-tail unit.

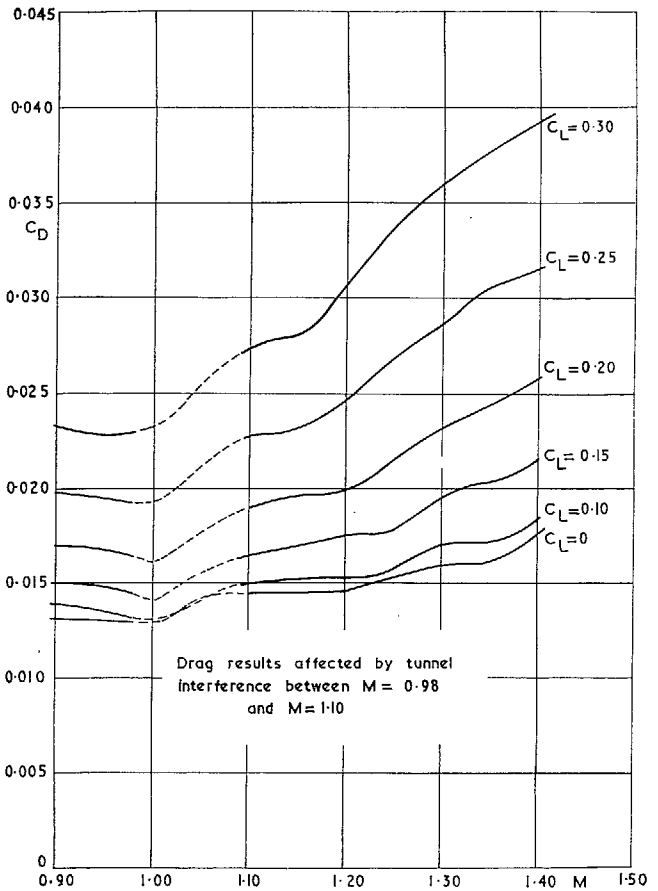

FIG. 3. Variation of C_D with M at constant C_L: model without fin-tail unit.

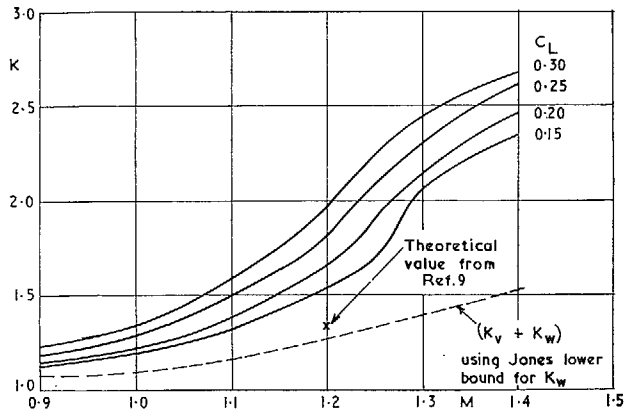

Typical values for C_L = 0·15

M	Experimental	Theoretical I	Theoretical II
0·9	1·13	1·078	1·078
1·2	1·55	1·28	1·335

For Theoretical I, K_w given by 'Jones lower bound'.
For Theoretical II, K_w derived from Ref. 9.
Experimental values are not based on $C_{D_{min}}$ but are an attempt to obtain values which should be combined with C_{D_0} for corresponding plane wing. (They are possibly somewhat optimistic — see Section 5.3)

FIG. 4. Variation of K with M and C_L: comparison with theoretical values.

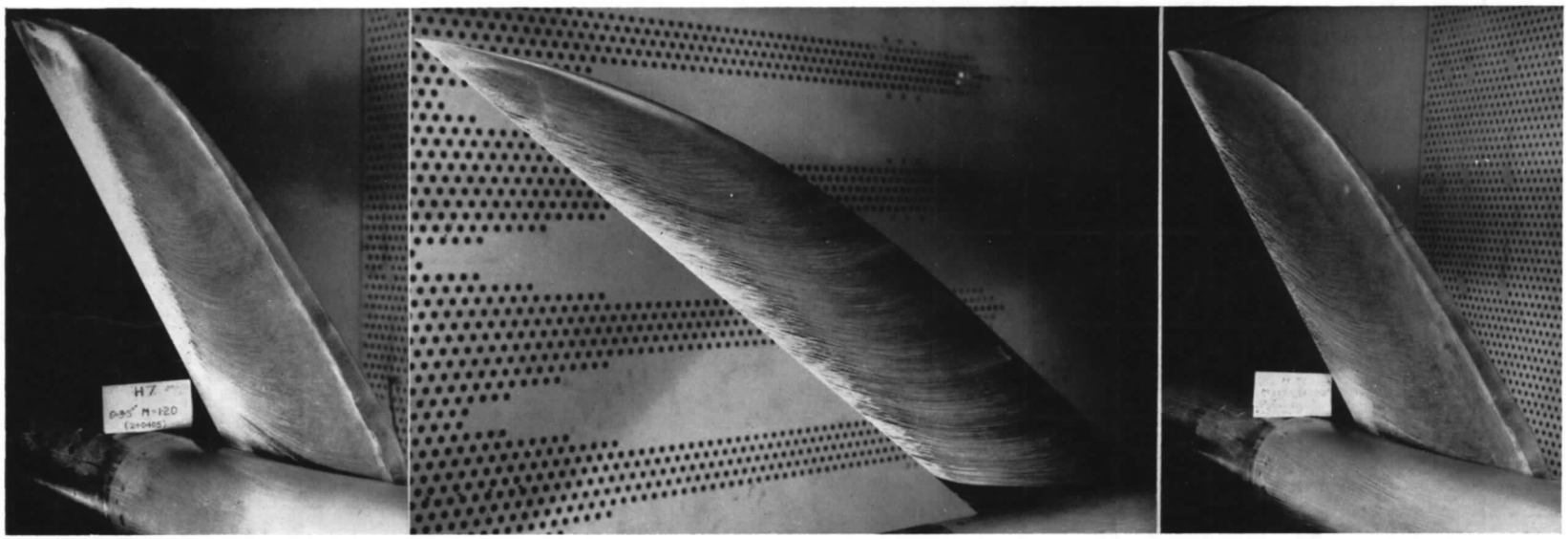

$C_L = 0{\cdot}20,\ M = 1{\cdot}20$ $C_L = 0{\cdot}15,\ M = 1{\cdot}20$ $C_L = 0{\cdot}135,\ M = 1{\cdot}25$

FIG. 5. Typical oil-flow photographs.

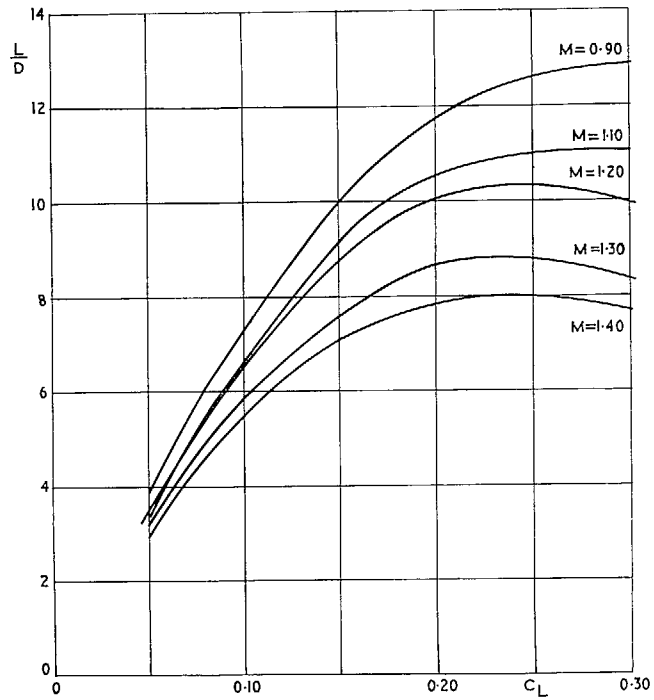

FIG. 6a. Variation of L/D with C_L and Mach number: Measured results for model without fin-tail unit.

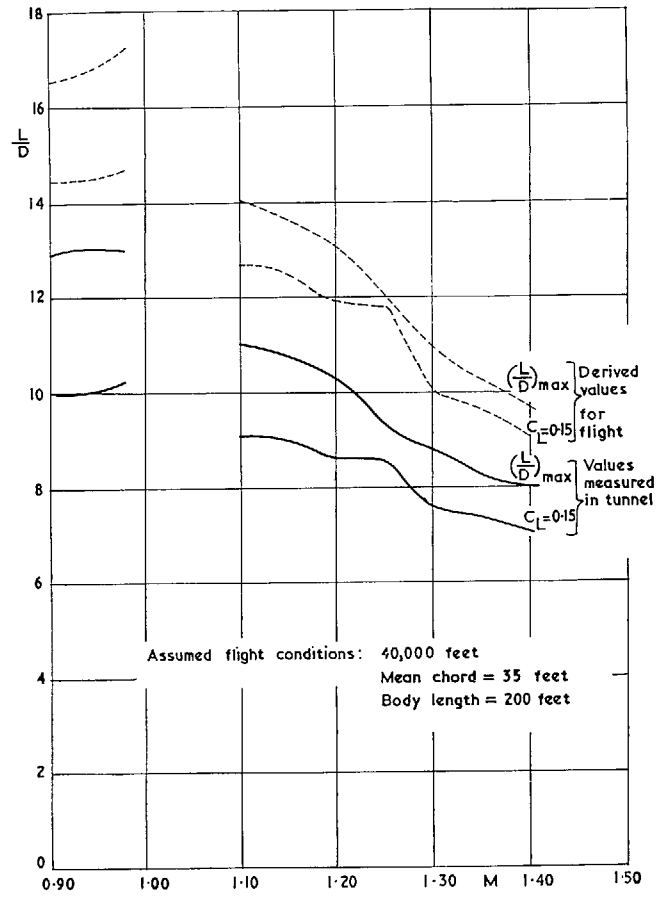

FIG. 6b. Variation of $(L/D)_{max}$ and typical cruise L/D with Mach number: Wing-fuselage; no fin-tail unit.

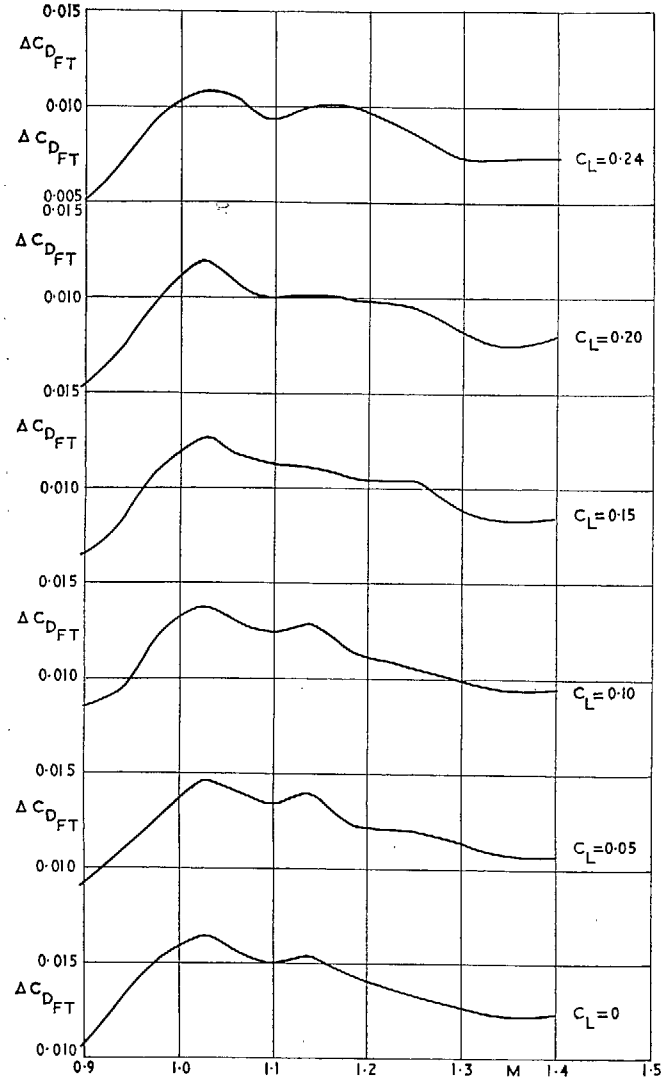

(a) $\eta_T = -6°30'$.

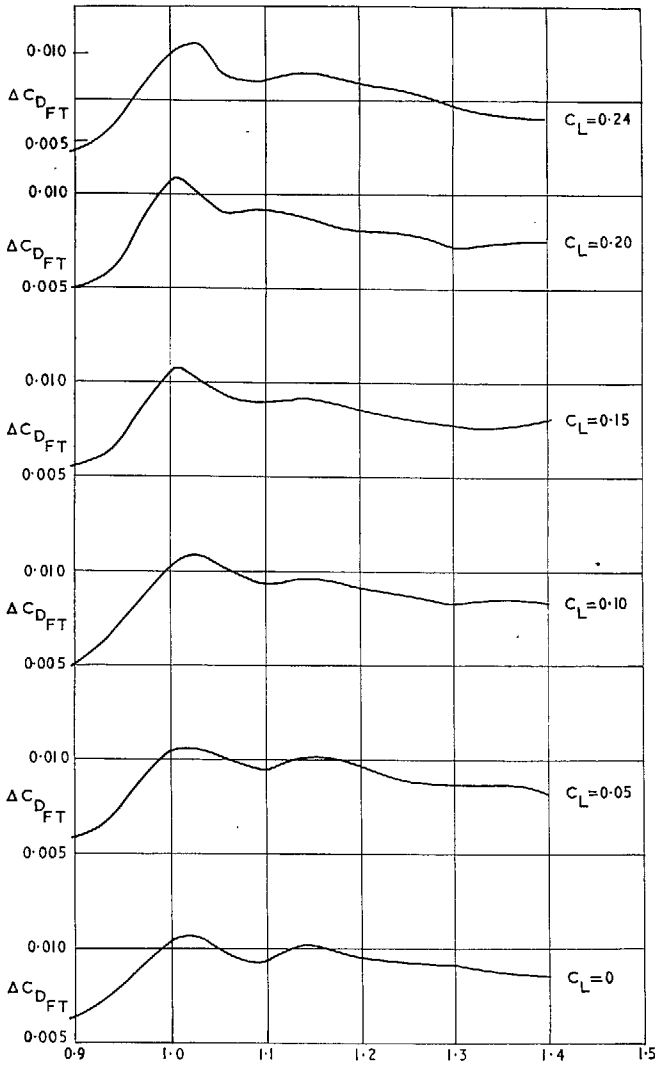

(b) $\eta_T = -2°49'$.

FIG. 7. Variation of tailplane and fin drag increments with Mach number.

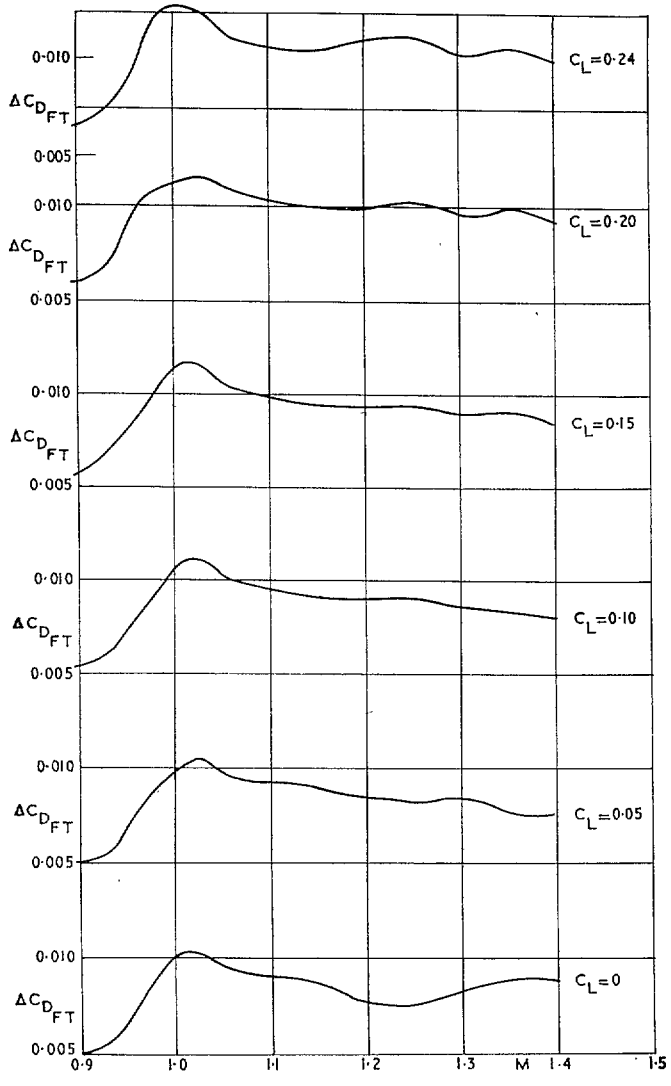

(c) $\eta_T = +\ 0°52'$.

FIG. 7. Variation of tailplane and fin drag increments with Mach number.

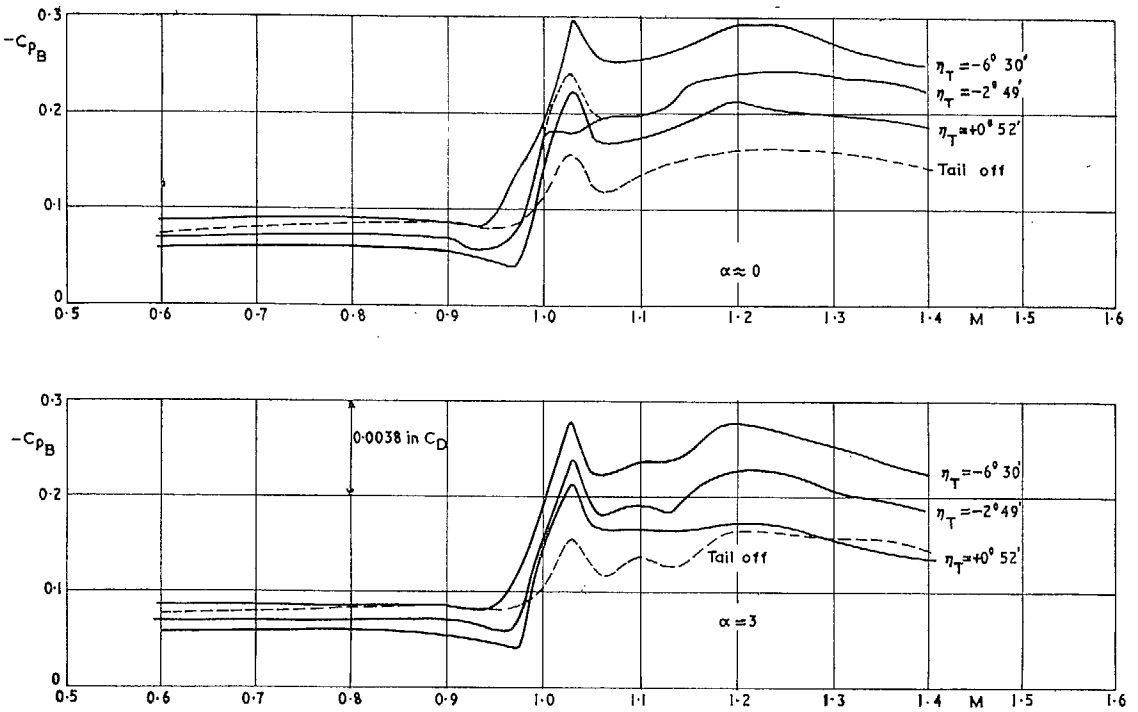

FIG. 8. Variation of base pressure with Mach number at various tail settings: $\alpha \approx 0$, $\alpha \approx 3$.

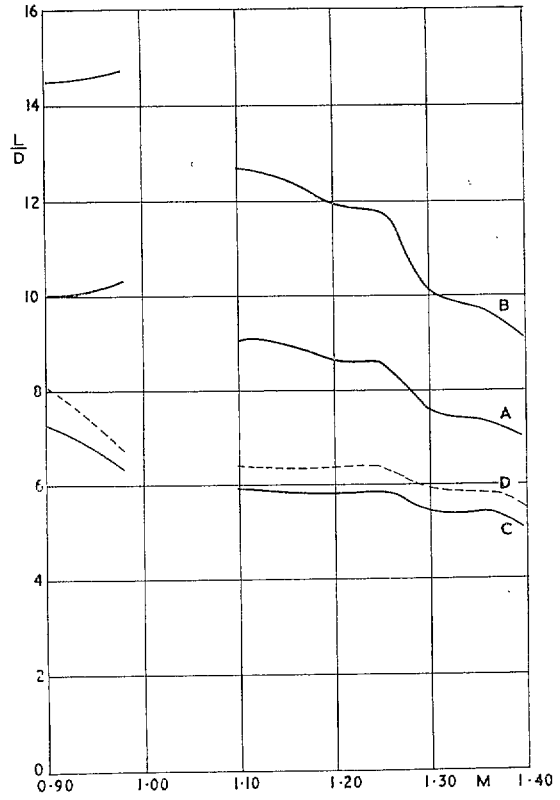

B: Tunnel values for wing-fuselage corrected to full-scale Reynolds number. ($R = 80 \times 10^6$)

A: Tunnel values for wing-fuselage. ($R \simeq 4{\cdot}3 \times 10^6$)

C: Tunnel values for complete model. ($R \simeq 4{\cdot}3 \times 10^6$)

D: Tunnel values for complete model, corrected to Reynolds number of free-flight tests. ($R = 10 \times 10^6$)

ie. (A − C) : Drag of fin-tail unit.

(C − D) : Effect of different R of tunnel and free-flight tests.

FIG. 9. Effect of fin-tail unit on L/D for $C_L = 0{\cdot}15$ (*see* Section 6).

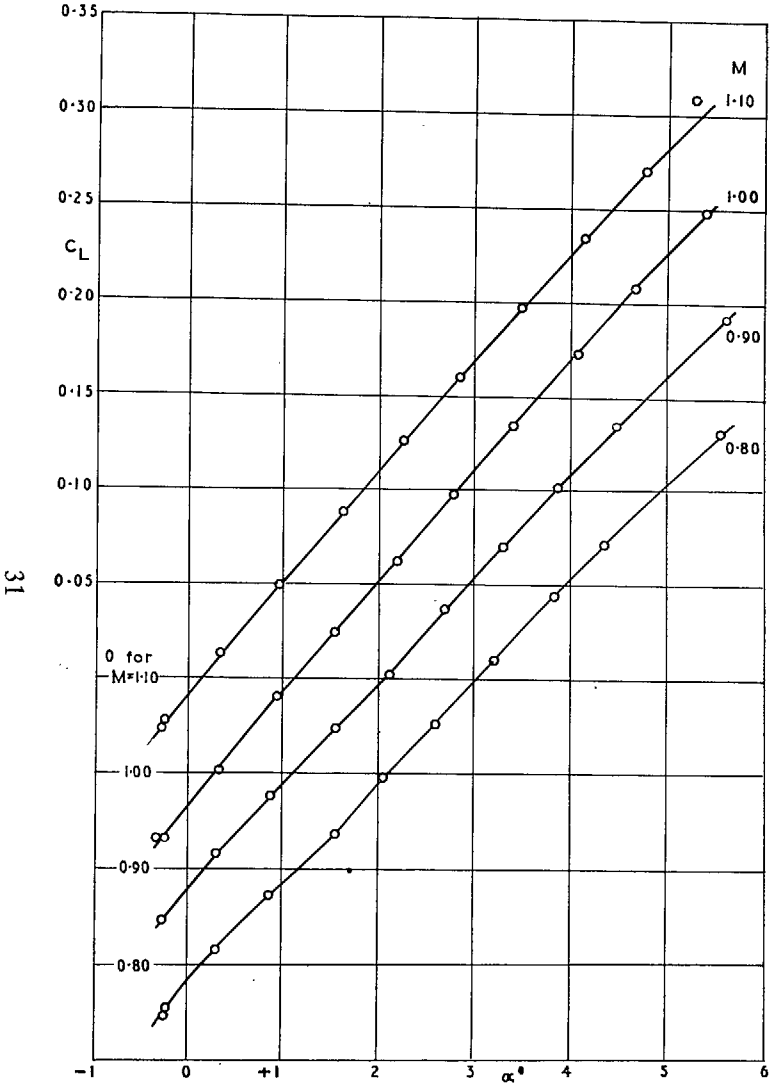

(a)

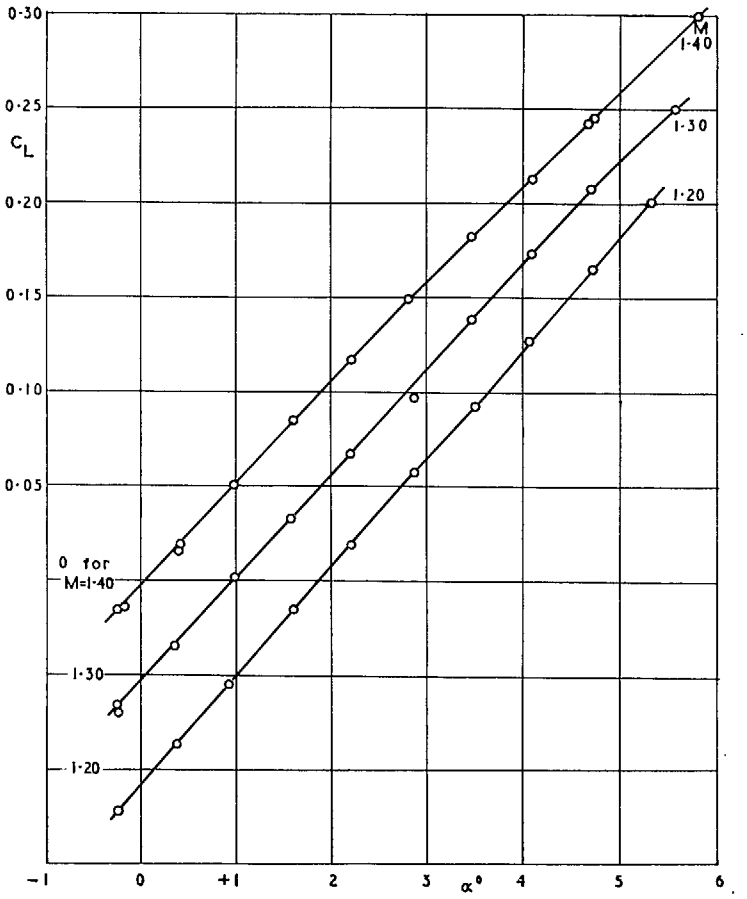

(b)

FIG. 10. Variation of C_L with α at constant Mach number.

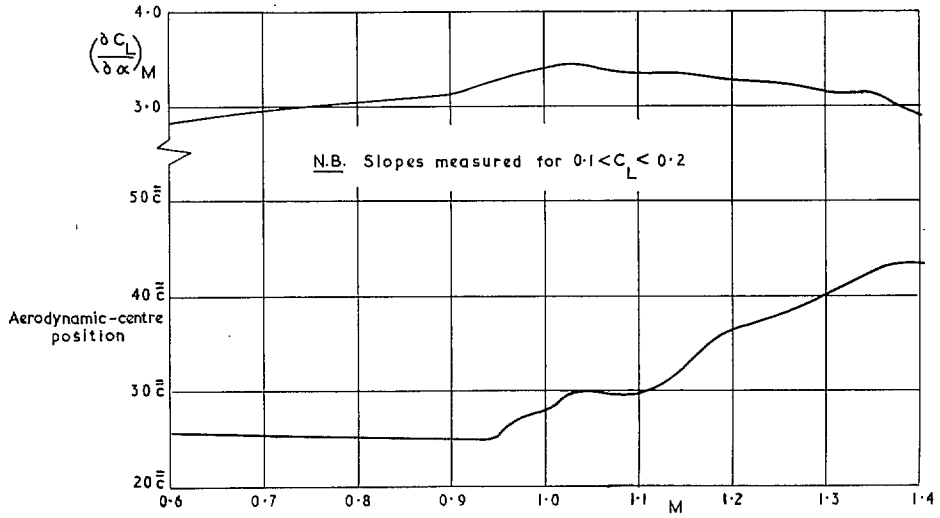

FIG. 11. Variation of lift-curve slope and aerodynamic-centre position with Mach number, tail off.

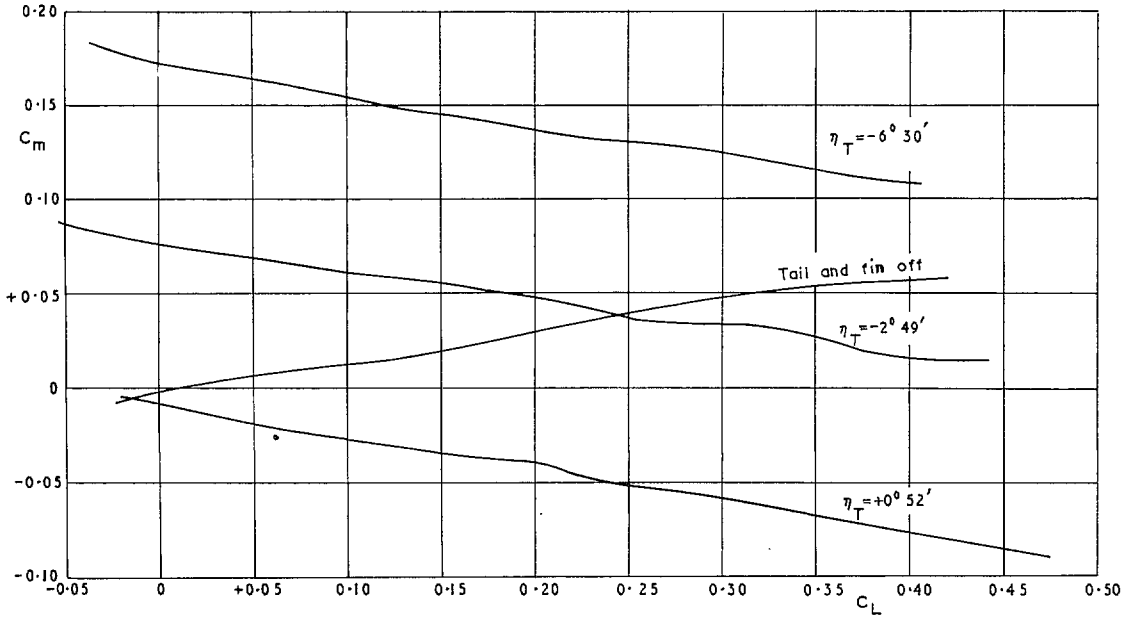

FIG. 12a. Variation of pitching moment with lift for $M = 0{\cdot}60$. Moment reference point $0{\cdot}4\bar{c}$.

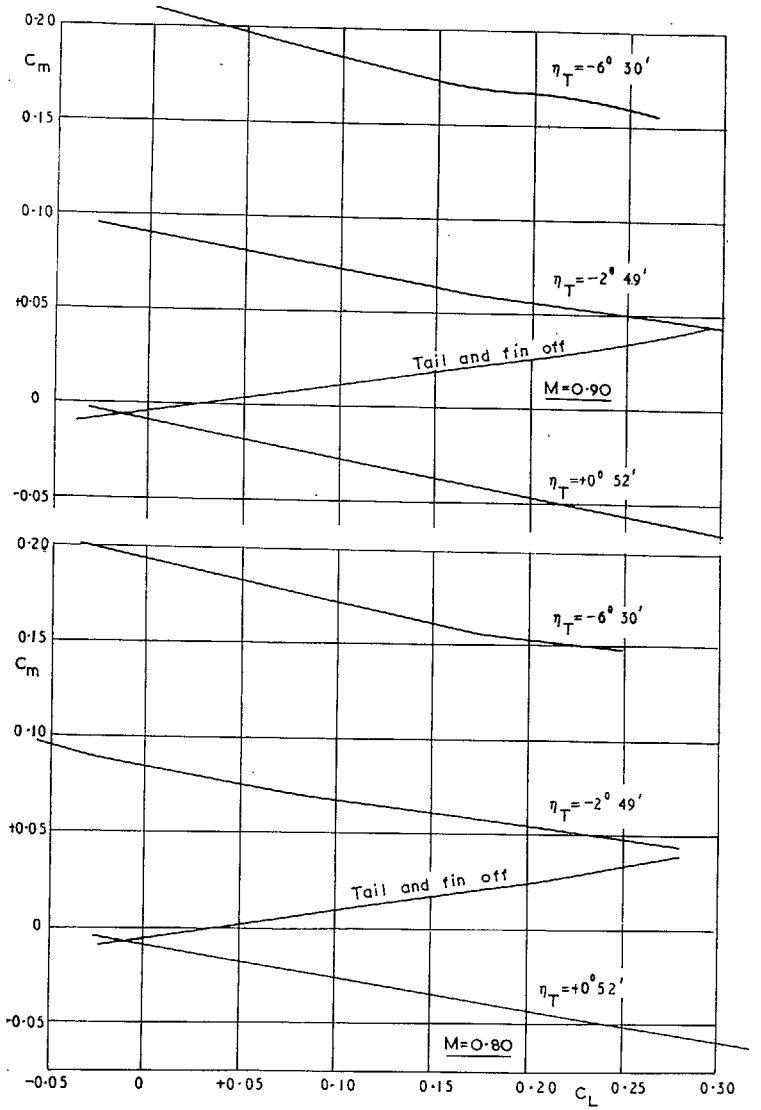

(b) $M = 0{\cdot}8$ and $0{\cdot}9$

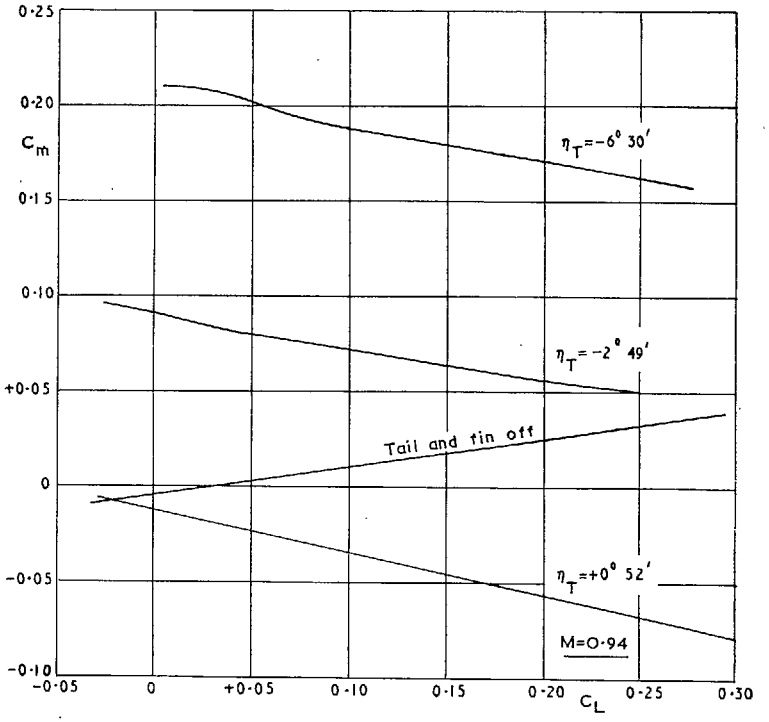

(c) $M = 0{\cdot}94$

FIG. 12. Variation of pitching moment with lift. Moment reference point $0{\cdot}4\bar{c}$.

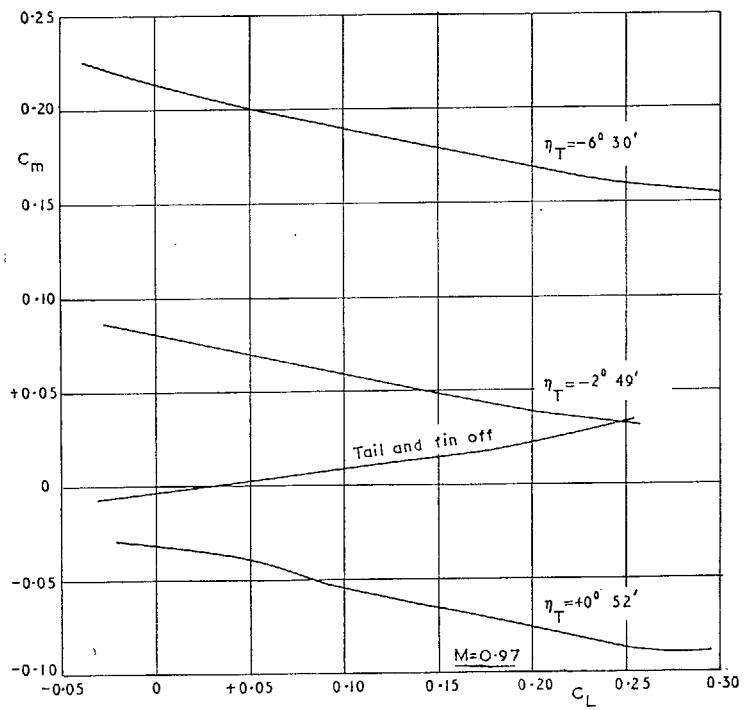

(d) $M = 0{\cdot}97$

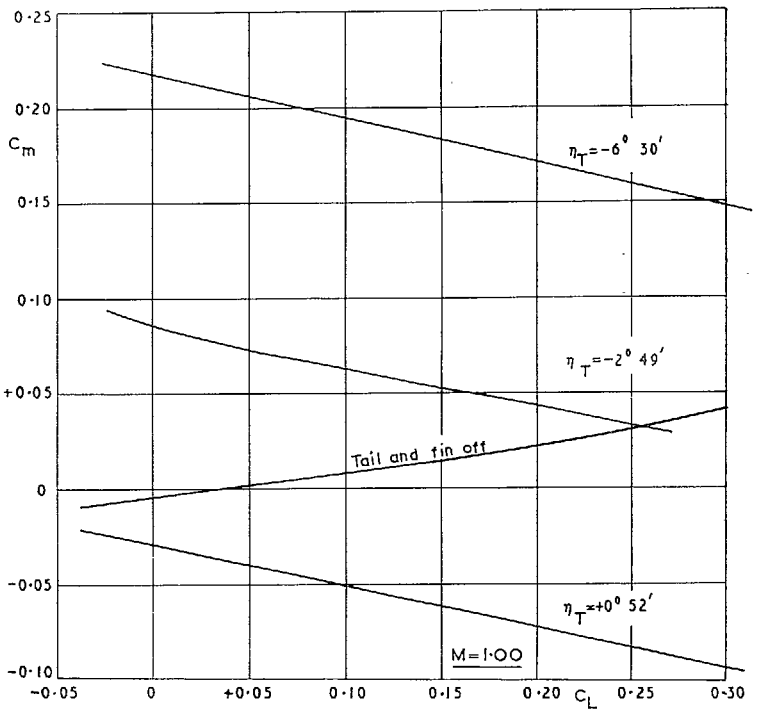

(e) $M = 1{\cdot}0$

FIG. 12. Variation of pitching moment with lift. Moment reference point $0{\cdot}4\bar{c}$.

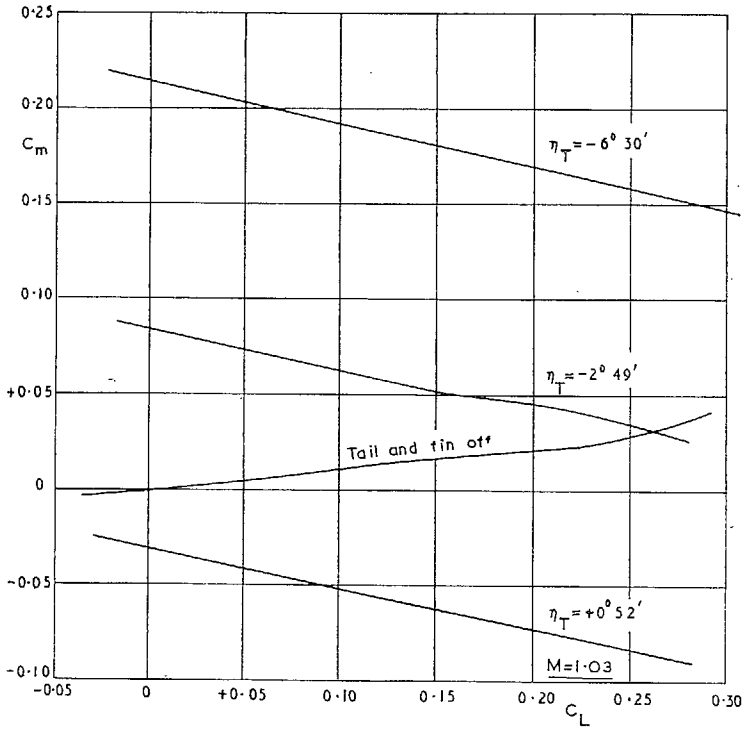

(f) $M = 1{\cdot}03$

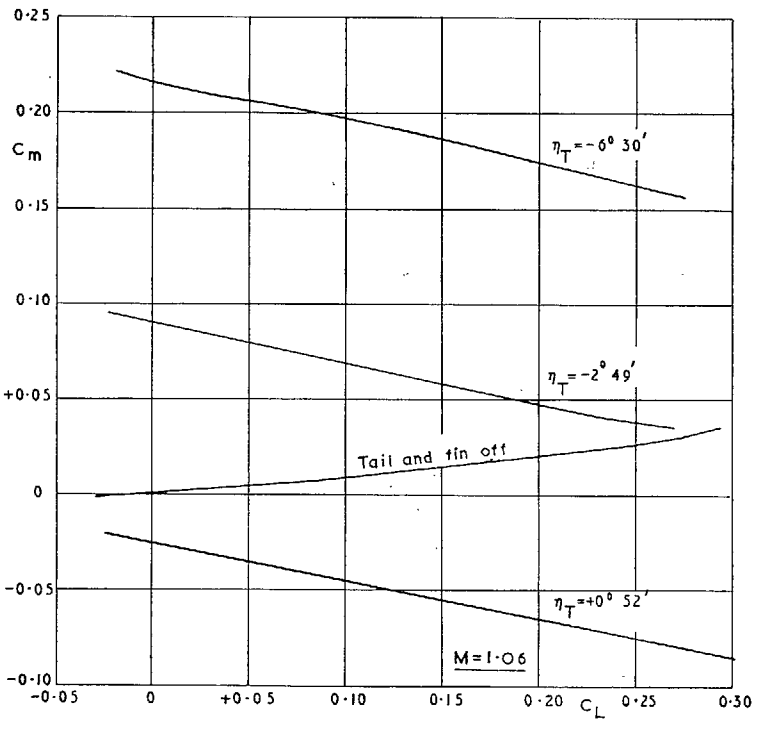

(g) $M = 1{\cdot}06$

FIG. 12. Variation of pitching moment with lift. Moment reference point $0{\cdot}4\bar{c}$.

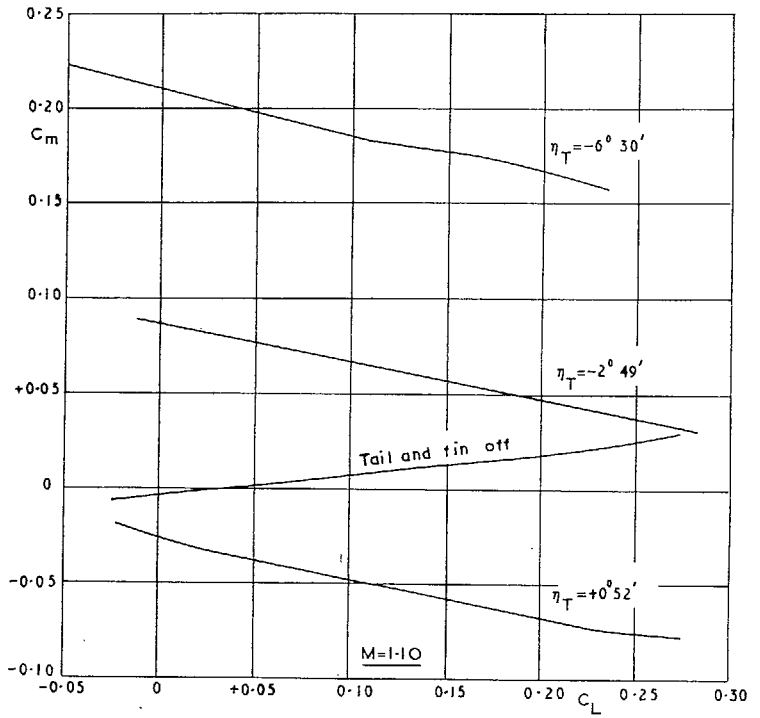

(h) $M = 1{\cdot}10$

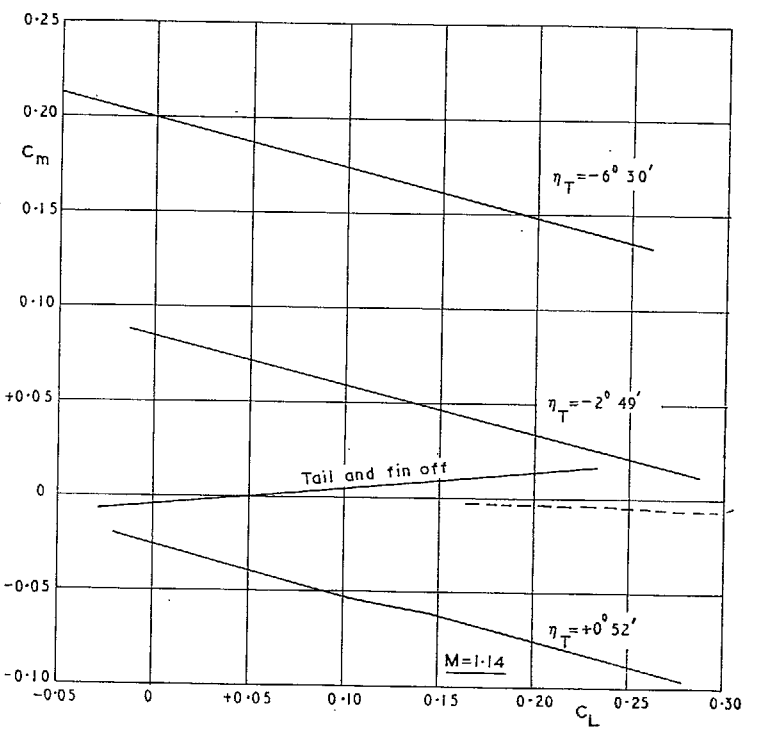

(j) $M = 1{\cdot}14$

FIG. 12. Variation of pitching moment with lift. Moment reference point = $0{\cdot}4\bar{c}$.

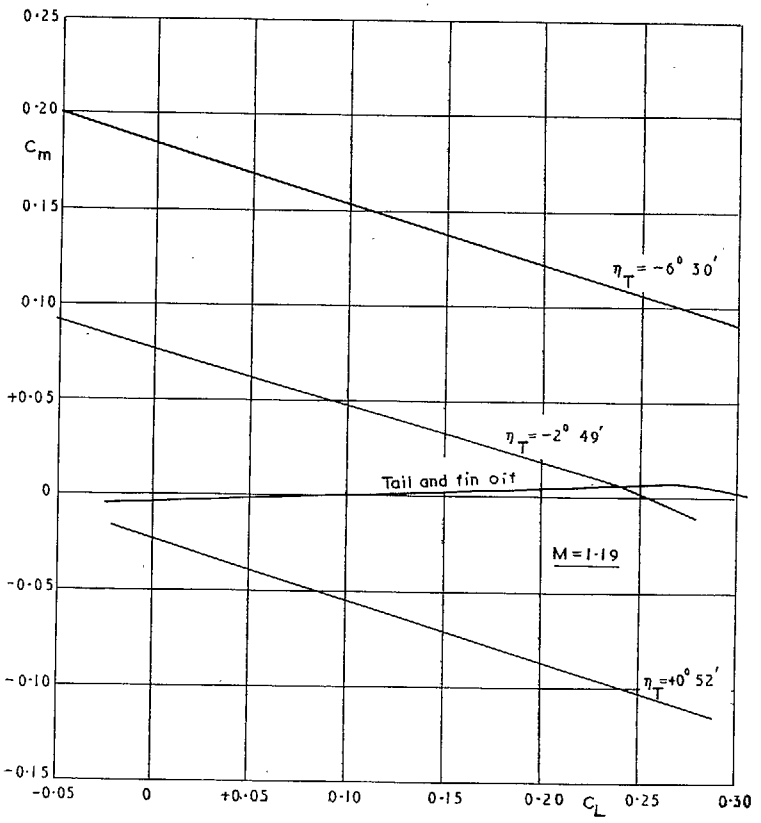

(k) $M = 1 \cdot 19$

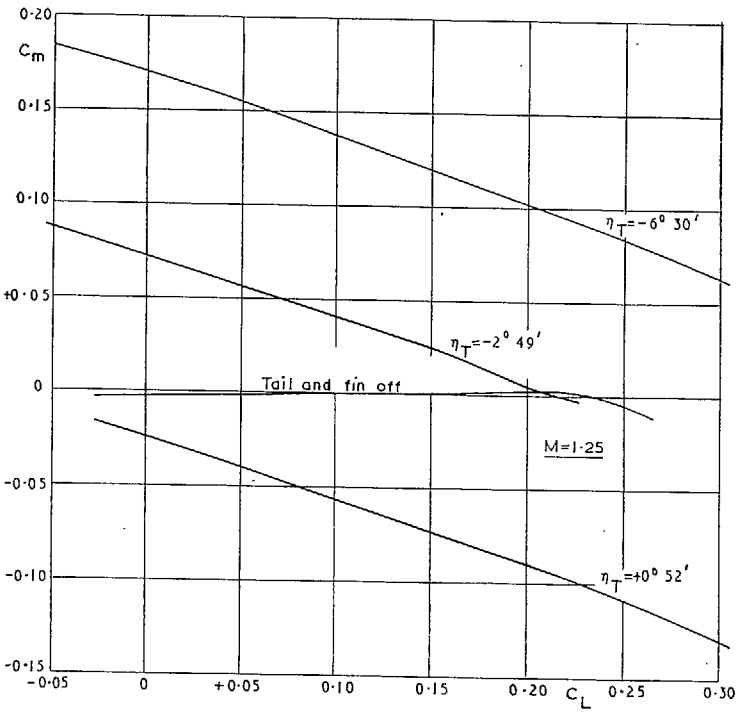

(l) $M = 1 \cdot 25$

FIG. 12. Variation of pitching moment with lift. Moment reference point = $0 \cdot 4\bar{c}$.

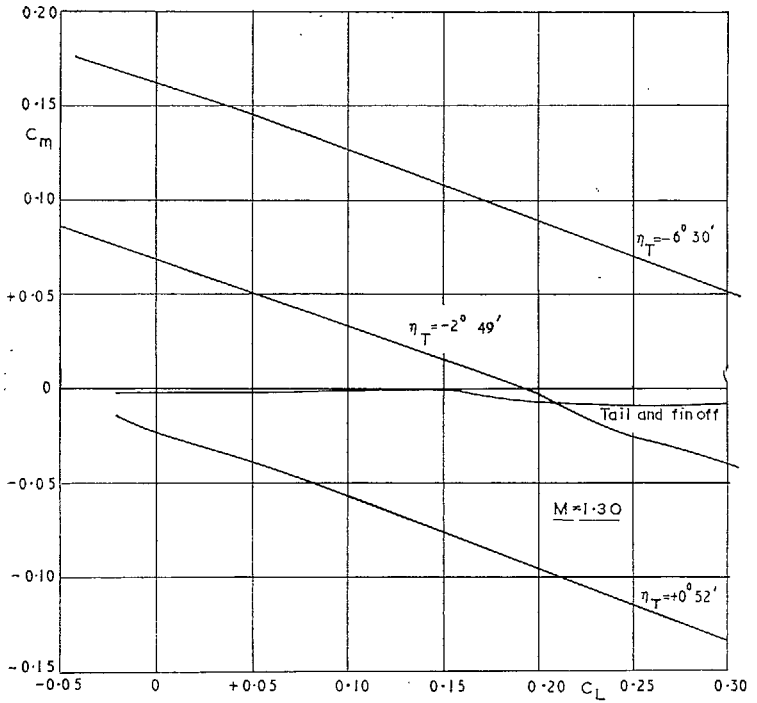

(m) $M = 1{\cdot}30$

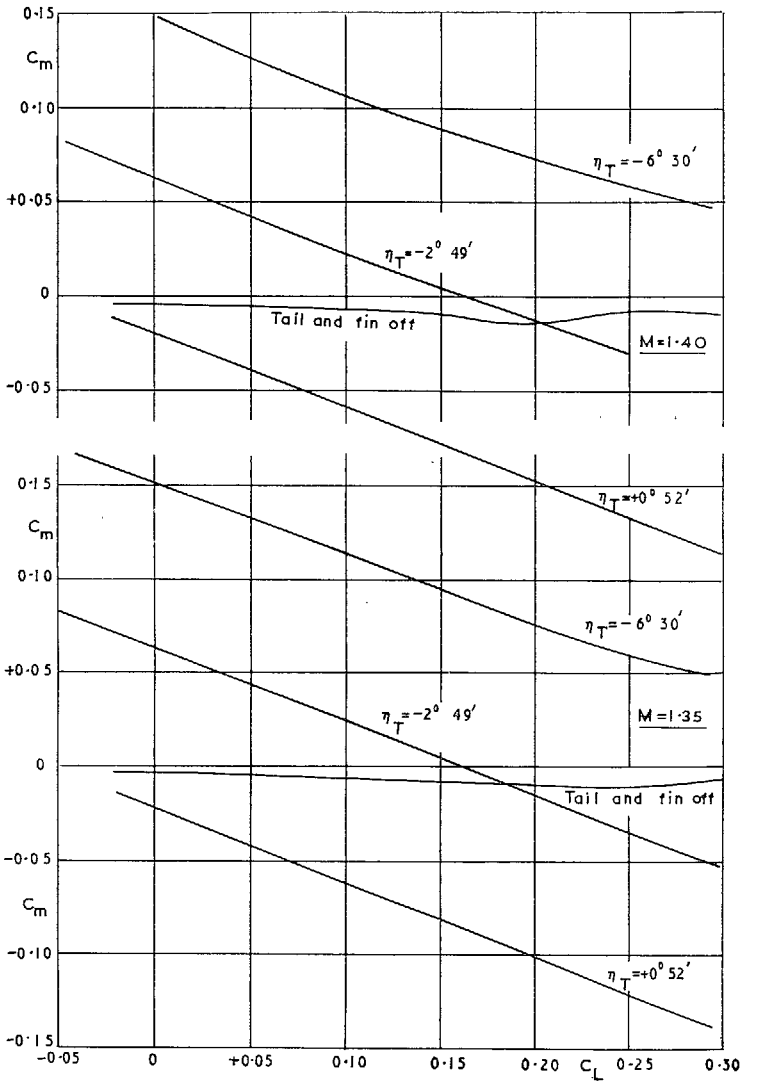

(n) $M = 1{\cdot}35$ and $1{\cdot}40$

FIG. 12. Variation of pitching moment with lift. Moment reference point = $0{\cdot}4\bar{c}$.

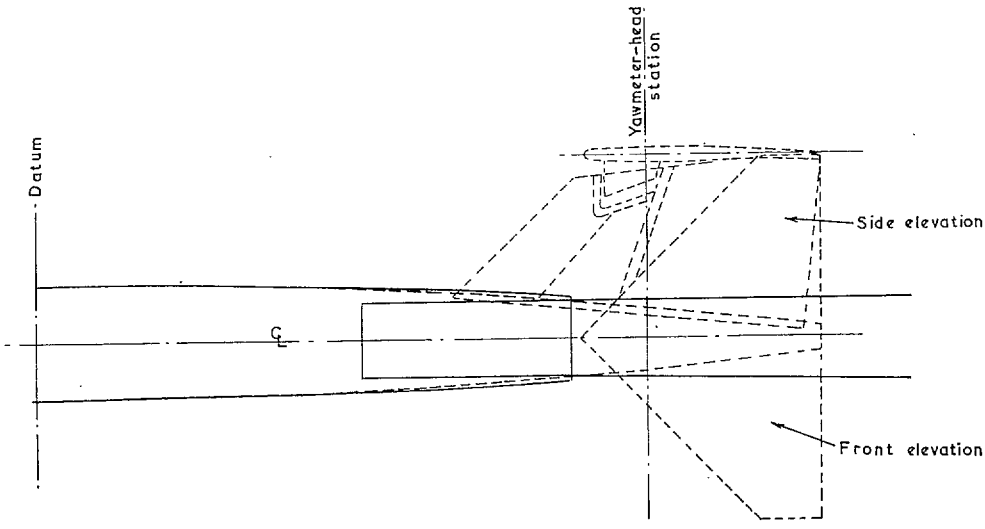

FIG. 13. Layout of rear end of plane-wing model for yawmeter test (scale: 1/8th model size).

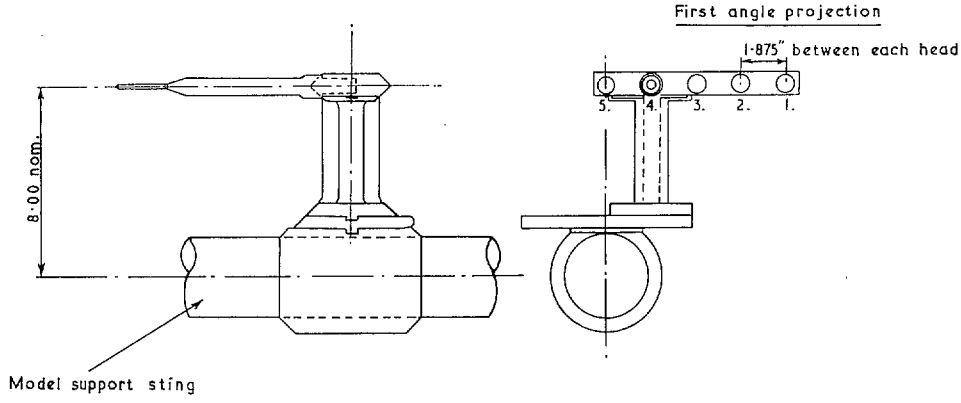

FIG. 14. Salient features of yawmeter comb for test with plane-wing model (scale: 1/8th model size).

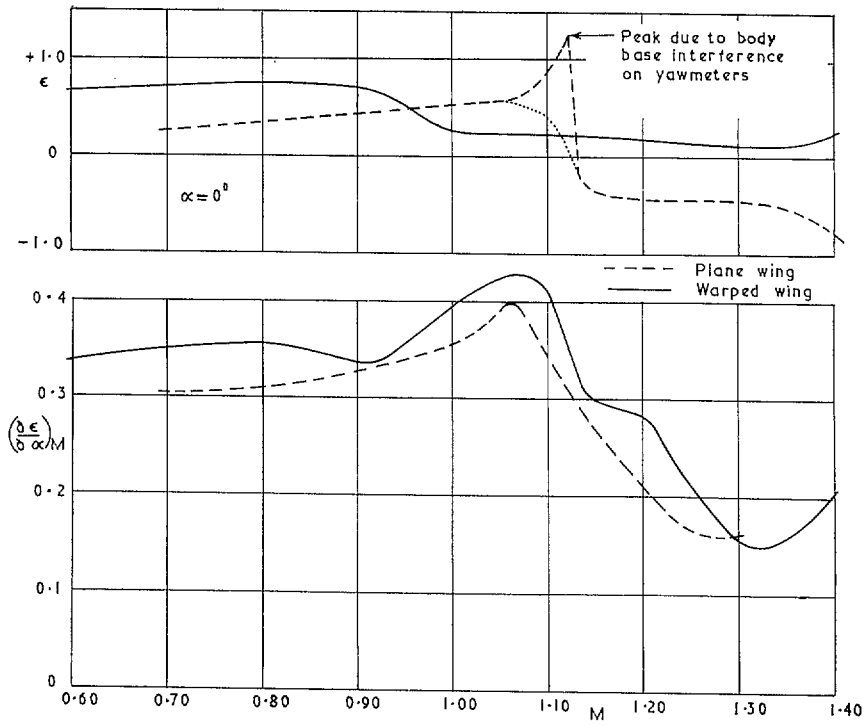

FIG. 15. Variation of downwash characteristics with Mach number.

(90632) Wt. 66/2301 K.5 11/64 Hw.

Publications of the Aeronautical Research Council

ANNUAL TECHNICAL REPORTS OF THE AERONAUTICAL RESEARCH COUNCIL (BOUND VOLUMES)

1942 Vol. I. Aero and Hydrodynamics, Aerofoils, Airscrews, Engines. 75*s.* (post 2*s.* 9*d.*)
Vol. II. Noise, Parachutes, Stability and Control, Structures, Vibration, Wind Tunnels. 47*s.* 6*d.* (post 2*s.* 3*d.*)

1943 Vol. I. Aerodynamics, Aerofoils, Airscrews. 80*s.* (post 2*s.* 6*d.*)
Vol. II. Engines, Flutter, Materials, Parachutes, Performance, Stability and Control, Structures. 90*s.* (post 2*s.* 9*d.*)

1944 Vol. I. Aero and Hydrodynamics, Aerofoils, Aircraft, Airscrews, Controls. 84*s.* (post 3*s.*)
Vol. II. Flutter and Vibration, Materials, Miscellaneous, Navigation, Parachutes, Performance, Plates and Panels, Stability, Structures, Test Equipment, Wind Tunnels. 84*s.* (post 3*s.*)

1945 Vol. I. Aero and Hydrodynamics, Aerofoils. 130*s.* (post 3*s.* 6*d.*)
Vol. II. Aircraft, Airscrews, Controls. 130*s.* (post 3*s.* 6*d.*)
Vol. III. Flutter and Vibration, Instruments, Miscellaneous, Parachutes, Plates and Panels, Propulsion. 130*s.* (post 3*s.* 3*d.*)
Vol. IV. Stability, Structures, Wind Tunnels, Wind Tunnel Technique. 130*s.* (post 3*s.* 3*d.*)

1946 Vol. I. Accidents, Aerodynamics, Aerofoils and Hydrofoils. 168*s.* (post 3*s.* 9*d.*)
Vol. II. Airscrews, Cabin Cooling, Chemical Hazards, Controls, Flames, Flutter, Helicopters, Instruments and Instrumentation, Interference, Jets, Miscellaneous, Parachutes. 168*s.* (post 3*s.* 3*d.*)
Vol. III. Performance, Propulsion, Seaplanes, Stability, Structures, Wind Tunnels. 168*s.* (post 3*s.* 6*d.*)

1947 Vol. I. Aerodynamics, Aerofoils, Aircraft. 168*s.* (post 3*s.* 9*d.*)
Vol. II. Airscrews and Rotors, Controls, Flutter, Materials, Miscellaneous, Parachutes, Propulsion, Seaplanes, Stability, Structures, Take-off and Landing. 168*s.* (post 3*s.* 9*d.*)

1948 Vol. I. Aerodynamics, Aerofoils, Aircraft, Airscrews, Controls, Flutter and Vibration, Helicopters, Instruments, Propulsion, Seaplane, Stability, Structures, Wind Tunnels. 130*s.* (post 3*s.* 3*d.*)
Vol. II. Aerodynamics, Aerofoils, Aircraft, Airscrews, Controls, Flutter and Vibration, Helicopters, Instruments, Propulsion, Seaplane, Stability, Structures, Wind Tunnels. 110*s.* (post 3*s.* 3*d.*)

Special Volumes

Vol. I. Aero and Hydrodynamics, Aerofoils, Controls, Flutter, Kites, Parachutes, Performance, Propulsion, Stability. 126*s.* (post 3*s.*)
Vol. II. Aero and Hydrodynamics, Aerofoils, Airscrews, Controls, Flutter, Materials, Miscellaneous, Parachutes, Propulsion, Stability, Structures. 147*s.* (post 3*s.*)
Vol. III. Aero and Hydrodynamics, Aerofoils, Airscrews, Controls, Flutter, Kites, Miscellaneous, Parachutes, Propulsion, Seaplanes, Stability, Structures, Test Equipment. 189*s.* (post 3*s.* 9*d.*)

Reviews of the Aeronautical Research Council

1939–48 3*s.* (post 6*d.*) 1949–54 5*s.* (post 5*d.*)

Index to all Reports and Memoranda published in the Annual Technical Reports

1909–1947 R. & M. 2600 (out of print)

Indexes to the Reports and Memoranda of the Aeronautical Research Council

Between Nos. 2351–2449	R. & M. No. 2450 2*s.* (post 3*d.*)
Between Nos. 2451–2549	R. & M. No. 2550 2*s.* 6*d.* (post 3*d.*)
Between Nos. 2551–2649	R. & M. No. 2650 2*s.* 6*d.* (post 3*d.*)
Between Nos. 2651–2749	R. & M. No. 2750 2*s.* 6*d.* (post 3*d.*)
Between Nos. 2751–2849	R. & M. No. 2850 2*s.* 6*d.* (post 3*d.*)
Between Nos. 2851–2949	R. & M. No. 2950 3*s.* (post 3*d.*)
Between Nos. 2951–3049	R. & M. No. 3050 3*s.* 6*d.* (post 3*d.*)
Between Nos. 3051–3149	R. & M. No. 3150 3*s.* 6*d.* (post 3*d.*)

HER MAJESTY'S STATIONERY OFFICE

from the addresses overleaf

Printed and published by
HER MAJESTY'S STATIONERY OFFICE

To be purchased from
York House, Kingsway, London W.C.2
423 Oxford Street, London W.1
13A Castle Street, Edinburgh 2
109 St. Mary Street, Cardiff
39 King Street, Manchester 2
50 Fairfax Street, Bristol 1
35 Smallbrook, Ringway, Birmingham 5
80 Chichester Street, Belfast 1
or through any bookseller

Printed in England

S.O. Code No. 23-3385